UNIVERSITY OF TWENTE.

Faculty of Electrical Engineering, Mathematics & Computer Science

Ion-Sensitive Gated Bipolar Transistor "ISBIT"

Sander E. J. Vincent

BSc Thesis

12 November 2018 - 1. February 2019

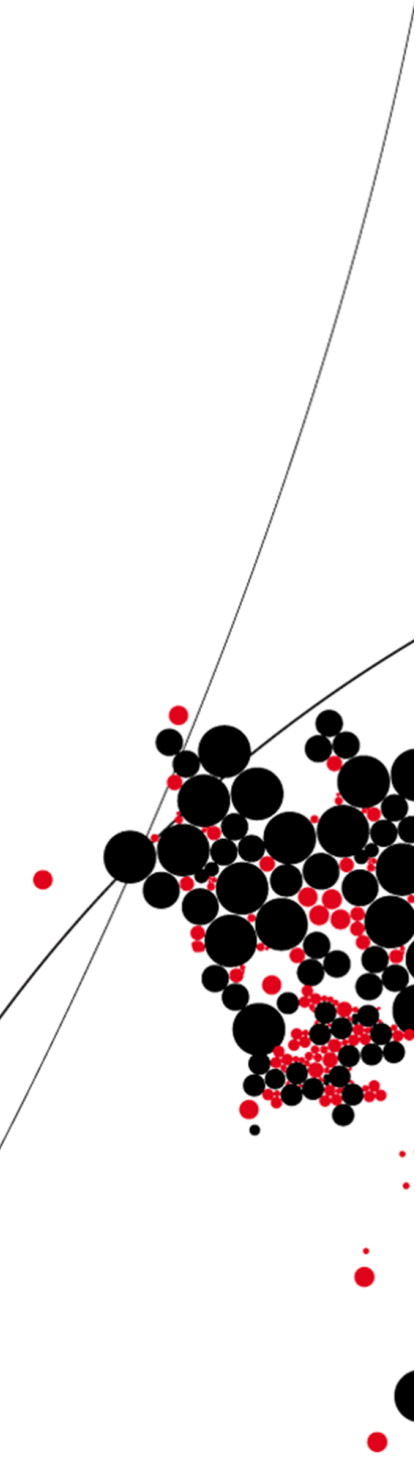

Supervisors:
dr. ir. R. J. E. Hueting
dr. ir. W. Olthuis
prof. dr. J. Schmitz

Group of Integrated Devices and Systems &
BIOS: Lab on a Chip Group
Faculty of Electrical Engineering,
Mathematics and Computer Science
University of Twente
P.O. Box 217
7500 AE Enschede
The Netherlands

Abstract

ISBIT is an acronym that stands for Ion Sensitive Gated Bipolar Transistor, which is the bipolar configuration, i.e. the emitter is supplied with a bias voltage, of the Ion Sensitive Field Effect Transistor (ISFET). It is assumed that in this configuration the output parameters can be improved without changing the method of measuring nor the structure of the ISFET. This introduces a research question on whether it is possible to increase the current and transconductance, or rather the sensitivity, when setting the ISFET in its bipolar mode to become the ISBIT.

At first, the theory behind the assumption is elaborated, where the clear distinctions and advantages are displayed. In the form of a current and a transconductance model a summary discusses what to expect from the simulations and the experiment itself. Following up on that are the TCAD simulations. Before evaluating the actual measurements, the setup and protocol are explained.

After processing both the current and transconductance in all operating regions, subthreshold, linear and saturation, and displaying the trends over all three pH values (4,7,10.01), it can be concluded that indeed the current and the transconductance improved to a certain extent. With this it is meant that both increased substantially in subthreshold and only minimally in saturation. In the linear operating region the current increased and so did the transconductance but only near the threshold voltage. Beyond the maximum transconductance, even a decrease was seen from ISBIT to ISFET. The general conclusion that can be drawn from this research is that the output parameters of an ISFET can be improved with the ISBIT configuration. This indicates that indeed the sensitivity of an ISFET can be increased in general terms.

Acknowledgement

First of all, I want to thank two members of my committee and my day-to-day supervisors Mr. Ray Hueting and Mr. Wouter Olthuis very much for the great support, help and advice I received from them over the span of this whole research. Additionally, for providing the necessary theory and technical guidance during the measurements in either of their respective fields. Also, I would like to thank Mr. Jurrian Schmitz, who represented the external committee member, allowed me to reserve the measuring devices in his name and lead me onto Mr. Remco Sanders. I would like to give special thanks to him as well, as he came up with the idea of- and also manufactured the custom box that made the ISFET measurements possible. Furthermore, special thanks to Mr. Johan Bomer who provided the MOSFETs and ISFETs and helped me acquire the chemical equipment for the ISFET measurements. Finally, thanks to the groups of IDS and BIOS for allowing me to use their equipment and to perform the measurements. Thank you very much to all, I am very grateful.

List of Acronyms

MOSFET	Metal Oxide Semiconductor Field Effect Transistor
MOSBIT	Metal Oxide Semiconductor BIpolar Transistor
ISFET	Ion Sensitive Field Effect Transistor
ISBIT	Ion Sensitive Gated Bipolar Transistor
ENFET	Enzyme Field Effect Transistor
IMFET	Immuno Field Effect Transistor
TCAD	Technology Computer-Aided Design
KITE	Keithley Interactive Test Environment
SMU	Source Measure Units
Si	Silicon
i.e.	id est
etc.	et cetera

List of Symbols

Symbol	Description	Unit
C_{Ox}	Areal Oxide Capacitance	$\frac{F}{m}$
g_m	Transconductance	$\frac{A}{V}$
I_{0C}	Prefactor Collector Current	A
I_{0D}	Prefactor Drain Current	A
I_C	Collector Current	A
I_D	Drain Current	A
L	Channel Length	m
m	Ideality Factor	
μ	Charge Carrier Mobility	$\frac{m^2}{(V \cdot s)}$
μ_T	Thermal Voltage	V
V_B	Body Potential	V
V_{BD}	Body-Drain Voltage	V
V_{BC}	Body-Collector Voltage	V
V_{BE}	Body-Emitter Voltage	V
V_{BS}	Body-Source Voltage	V
V_C	Collector Potential	V
V_{CE}	Collector-Emitter Voltage	V
V_D	Drain Potential	V
V_{DS}	Drain-Source Voltage	V
V_E	Emitter Potential	V
V_{GB}	Gate-Bulk Voltage	V
V_{GE}	Gate-Emitter Voltage	V
V_{GS}	Gate-Source Voltage	V
V_{Ref}	Reference Voltage	V
V_{pH}	Voltage depending on the pH value of the solution	V
V_S	Source Potential	V
V_{Th}	Threshold Voltage	V
W	Channel Width	m

Contents

Chapter 1

Introduction

In 1970 Piet Bergveld proposed and realized the first Ion Sensitive Field Effect Transistor (ISFET) which classifies as a potentiometric chemical sensor and can be used for example to sense ions within a solution and in turn determine the ionic concentration. [1] [2] Over the past 50 years this specific sensor has been improved, innovated and reinterpreted as there exist many versions for different purposes, like for example the ENFET or IMFET. [3] In this research, the particular Ion Sensitive Gated BIpolar Transistor, abbreviated ISBIT, is analyzed and it describes an ISFET in its bipolar configuration.

1.1 Motivation

A typical ISFET measures the ions present in an electrolyte through the help of its oxide that is very susceptible to ions and a reference electrode that transfers a potential onto this aqueous solution. If a specific threshold voltage is surpassed within the device a current will start to flow and with the help of this output, called the transconductance, the variation of output current to input voltage, the ion concentration can be determined. [2] Now, if this current or transconductance could be increased under the same conditions by only switching the ISFET to the ISBIT, it would simplify and improve the assessment and determination of the ion concentration. Basically, enhancing the sensitivity from the reference electrode to the interaction with the ions at the interface to the output current of the transistor. Obviously, doing so without changing anything to the method of measurement nor the structure of the ISFET. So, ISFETs will have to be compared with ISBITs for various pH values to see whether there is an actual improvement, if this improvement is significant enough and, finally if it were to be, to recognize a trend.

1.2 Framework

On the basis of a study about innovative ion sensitive devices within the same group of IDS at the University of Twente, the, as mentioned in the document, ISBIT was claimed to have an improved transconductance in comparison with the ISFET. [4] Furthermore, prior to starting this research, already, there were some simulations performed that supported this claim. [5] Additionally, though this research wasn't carried out at the University of Twente, it is already known that for a lateral bipolar junction transistor within a MOSFET structure, the current gain and open circuit voltage outperform the typical MOSFET. [6]

1.3 Goal(s) of the assignment/Research question(s)

An overall aim of this research is an enhancement in the area of ion sensing. Generally, a goal from an experimental point of view is a distinct practical comparison of the ISBIT with ISFET. And specifically, an objective would be to improve sensitivity in the application of ion sensing. The particular research questions can be formulated as:

- Can the sensitivity, i.e the output current or rather the transconductance, with the help of an ISBIT be improved in comparison to an ISFET?

1.4 Report organization

The remainder of this report is organized as follows. Chapter 2 will elaborate on the theory behind the research. It does so by going through the basic theory of a MOSFET as both devices, ISFET and ISBIT, are based on this. Then, the distinctive properties of these transistors will also be elucidated. The chapter following up on that will show the TCAD simulations results performed with the actual ISFET structure. After that, in Chapter 4, the focus is on explaining the setup and the procedure of each measurement. Finally, in Chapter 5 the actual results of the ISFET and ISBIT measurements are presented, described and discussed. The report ends with Chapter 6, in which conclusions are drawn and recommendations are made.

Chapter 2

Theory

The intention of this chapter is to elaborate on the configuration and the working principle of three of the four to be analyzed transistors, namely the MOSFET, ISFET and ISBIT. The explanation of the devices will only contain the basic and relevant principles. Moreover, the important mathematical expressions are also described. For background information on the MOSFET theory or generally semiconductor physics basics such as drift, diffusion, generation, recombination and lattice structures etc. refer to [7] and [8]. If more needs to be known about the ISFET and ISBIT then refer to [2], [3], [4], [9] and [10]. Chapter 2 starts off by describing the basic functionality of a traditional MOSFET. After that, the difference between the ISFET and MOSFET will be clarified. This is followed by the distinction between ISBIT and ISFET. The chapters' final section contains a small derivation or rather a summary for what to expect in the simulations and the measurements.

2.1 Metal Oxide Semiconductor Field-Effect Transistor

The abbreviation MOSFET is explained first. MOS stands for Metal, Oxide and Semiconductor respectively. The metal part refers to the material used for the terminals. The oxide is a specific insulator that isolates the gate from the body. Finally, the main body is the semiconducting part which normally contains differently doped areas. The aforementioned insulator is grown on top of the semiconducting body. [7] The FET is an acronym for field-effect transistor and can be ascribed to the fact that this device is basically a switch of which the resistance is controlled, between the two terminals of source and drain, with an applied voltage on the gate, ultimately creating an electric field from gate to body. [7] Essentially, this implies that it can be seen as a voltage controlled current source. [8] As previously stated, there are doped regions, that can be classified as either n or p, which is the number of free

electrons and free holes, respectively. The semiconducting regions of the source and drain have the same kind of doping and the bulk has the opposite doping of those two. A cross-section of the MOSFET can be seen in figure 2.1. [8]

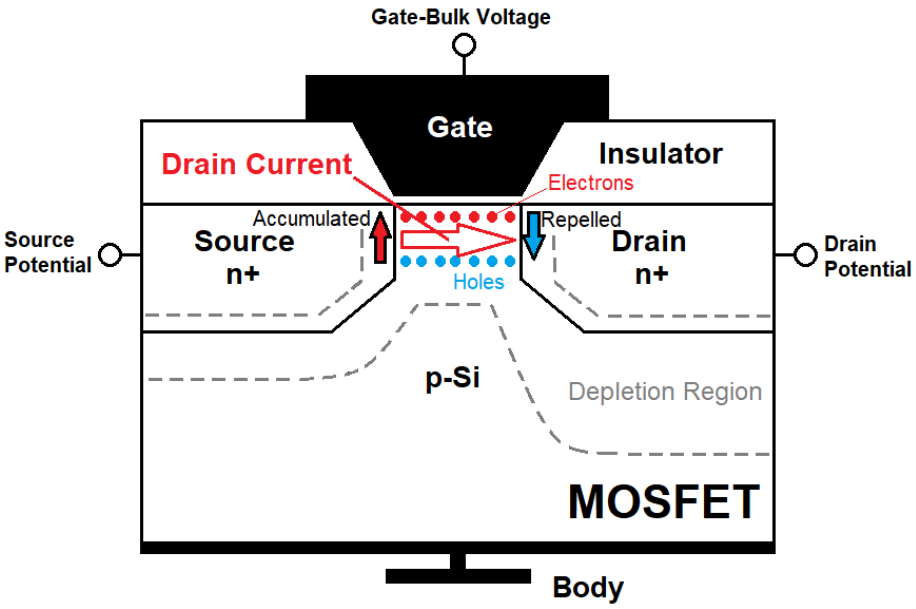

Figure 2.1: Cross-sectional view of a MOSFET.

To describe the MOSFETs' functionality an n-type structure and a ground on the body contact are assumed. The current through the transistor flows from the drain to the source. This can be achieved by altering the gate voltage, that will be referred to as gate-bulk voltage. Generally, if a sufficiently high, i.e exceeding a certain threshold, gate-bulk voltage is supplied then it ultimately repels the holes right underneath the oxide in the p-doped body and accumulates electrons to create a conducting channel. This conducting channel allows electrons to pass the body from source to drain, thereby inducing a current, which will be referred to as the drain current. The fact that this current is only carried by electrons, makes the MOSFET a unipolar device. [7] [8]

Not only can the current flowing from drain to source be influenced by the gate-bulk voltage, but also by applying a bias voltage to the drain, source or both (referred to as the drain potential and source potential; the total voltage across both contacts is the drain-source voltage). Depending on the gate-bulk voltage and drain potential, the transistor invokes different operating regions. The four being linear, saturation, cut-off/subthreshold and breakdown region. All these operating regions and their sequential arrangement can be observed in figure 2.2. In all these regions, the output current and the transconductance are specifically adjusted and, hence, have to be defined separately. [7]

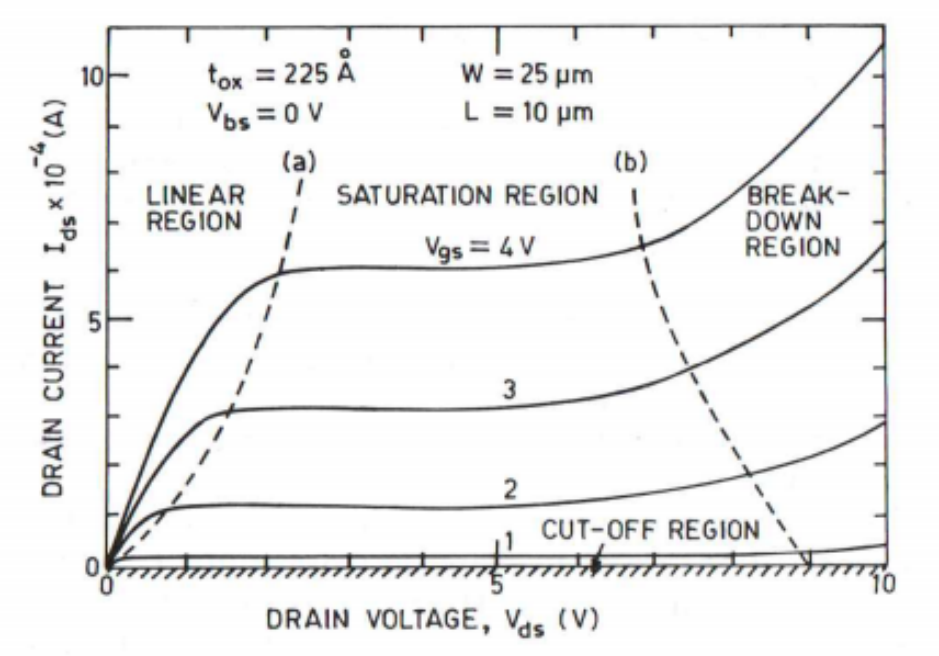

Figure 2.2: Operating regions of a typical MOSFET. [7]

The cut-off range, also referred to as subthreshold region, is the region below the threshold voltage. Here, there is no conducting channel between source and drain, but there could still be a leakage current ($V_{GB} < V_{Th}$). [7] The current

$$I_D = I_{0D} \cdot e^{\frac{V_{GS}-V_{Th}}{m\mu_T}} \cdot \left(1 - e^{-\frac{V_{DS}}{\mu_T}}\right), \qquad [A] \tag{2.1}$$

describes the full output within this range. The first to occur superthreshold region ($V_{GB} > V_{Th}$) is the linear operating region with its output current defined as

$$I_D = \mu C_{Ox} \cdot (\frac{W}{L}) \cdot (V_{GS} - V_{Th} - \frac{1}{2} \cdot V_{DS}) \cdot V_{DS}, \qquad [A] \tag{2.2}$$

that describes a drain voltage range that makes the drain current increase linearly with this voltage. [7] Saturation implies,

$$I_D = \frac{1}{2} \cdot \mu C_{Ox} \cdot (\frac{W}{L}) \cdot (V_{GS} - V_{Th})^2, \qquad [A] \tag{2.3}$$

that the drain voltage is so high, the drift velocity of the electrons saturates. The charge carriers can't flow any faster than that specific velocity due to the high lateral electric field and so is not dependent on this parameter, V_{DS}, anymore. [7] Lastly, the breakdown voltage, which literally causes the device to break down, because the voltage is too high for the transistor to cope with. [7] For this research the breakdown voltage is of no interest.

Now, generally the transconductance can be summarized as

$$g_m = \frac{dI_D}{dV_{GS}}. \qquad [A/V] \tag{2.4}$$

This variation of the output current to variation of the input voltage has the following effect on the transconductance in each operating region,

$$g_m = \frac{I_{0D}}{m\mu_T} \cdot e^{\frac{V_{GS}-V_{Th}}{m\mu_T}} \cdot \left(1 - e^{-\frac{V_{DS}}{\mu_T}}\right), \qquad [A/V] \tag{2.5}$$

$$g_m = \mu C_{Ox} \cdot (\frac{W}{L}) \cdot V_{DS} \qquad [A/V] \tag{2.6}$$

and

$$g_m = \mu C_{Ox} \cdot (\frac{W}{L}) \cdot (V_{GS} - V_{Th}) \qquad [A/V] \tag{2.7}$$

representing, from (2.5) to (2.7), the subthreshold-, linear- and saturation operating region.

2.2 Ion Sensitive Field Effect Transistor

ISFET is an abbreviation for ion sensitive field effect transistor. [2] Hence, the term FET still implies the same thing as previously described in section 2.1. Generally, considering the working principle of the MOSFET in the previous section, the ISFETs' functionality is comparable. The only thing that has changed structure-wise is the gate terminal. Instead of having direct contact with the insulating layer, the gate is now represented by a reference electrode released from the rest of the transistor, leaving the oxide surface exposed. [2] The entirety consisting of a mounted ISFET and the reference electrode is submerged into an aqueous solution with a certain pH value and hence a certain number of ions and allows the ion-sensitive (I and S in the acronym) oxide layer to be in direct contact with this buffer. The reference electrode determines the potential of this buffer and ultimately causes charge modulation at the oxide surface of the ISFET. [2] [3] Hence, the actual supplied gate-bulk voltage will deviate because of these components. This can be summarized as

$$V_{GB} = V_{Ref} + V_{pH} + Constant \qquad [V] \tag{2.8}$$

which can be substituted into the current and transconductance equations for consideration of the pH sensitivity. In general, this is still very much comparable to a normal bias voltage on the gate of a MOSFET, as described in 2.1, because just as before, a bias voltage will induce a conducting channel in the device. Here, charge carriers in the semiconducting body will be influenced by the ionic charge in the solution across the oxide and cause a current to flow from drain to source. So, the

information of the aqueous solution is transduced from the chemical to the electrical domain. [2] A schematic coupled with the described occurrences regarding an ISFET is shown in figure 2.3. The operating regions, also mentioned in the MOSFET theory section 2.1, are still applicable.

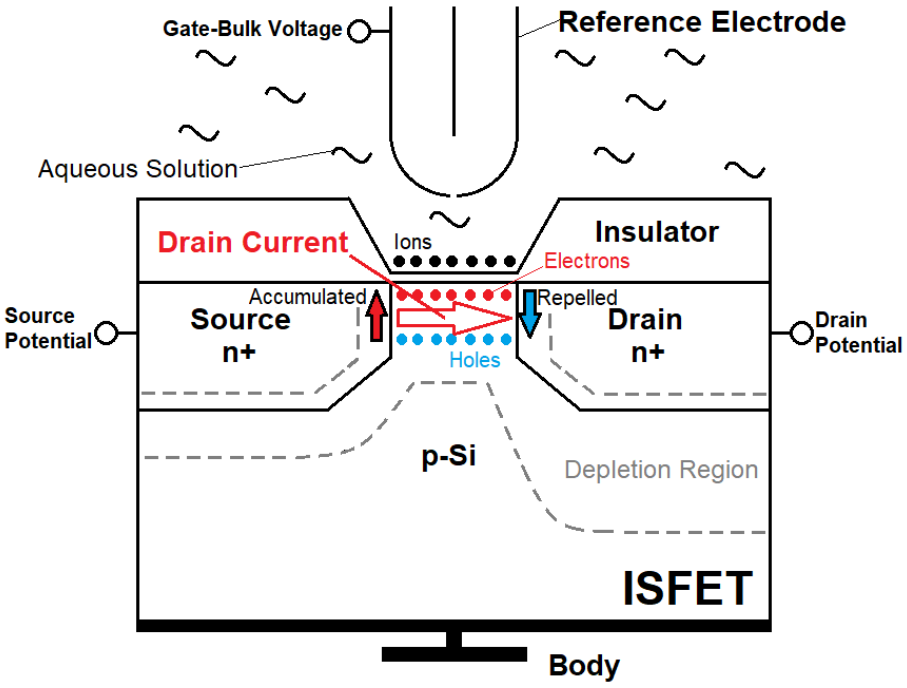

Figure 2.3: Cross-Sectional View of an ISFET

2.3 Ion Sensitive Gated BIpolar Transistor

In the Ion Sensitive Gated Bipolar Transistor configuration nothing is different from the ISFET in terms of structure. The working principle, however, now changes to the distinctive bipolar mode, in which the first two letters represent Bi in the abbreviation. In 2.1, the effects and the corresponding operating regions, when altering the gate-bulk and drain potential were elaborated. Now, it is the source or rather the emitter bias voltage that plays the important role. To differ between the two modes, the source and drain contacts are now going to be referred to as emitter and collector contacts. This is as soon as the source potential is not equal to zero anymore, then it becomes the emitter potential. [10] For the n-type transistor that is still assumed, this emitter potential has to be negative to fulfill the desired outcome. So, when this emitter bias voltage is applied it introduces new currents that will influence the collector current. First of all, the collector current, electrons flowing from emitter to collector through the conducting channel, equivalent to the previous drain current, is obviously present. But it can be seen that there will be a second current flowing

from emitter to collector. However, it will flow mainly through the bulk, making this the collector-bulk current. [4] Furthermore, this emitter potential produces an injection of holes from the body into the emitter and electrons from the emitter to the body, invoking a diode relation between the two terminals. [10] This significant emitter-body current, will also influence the eventual emitter current. Because of the fact that both charge carriers are actively present, this device is bipolar. A schematic of the ISBIT together with the various described currents flowing can be seen in figure 2.4.

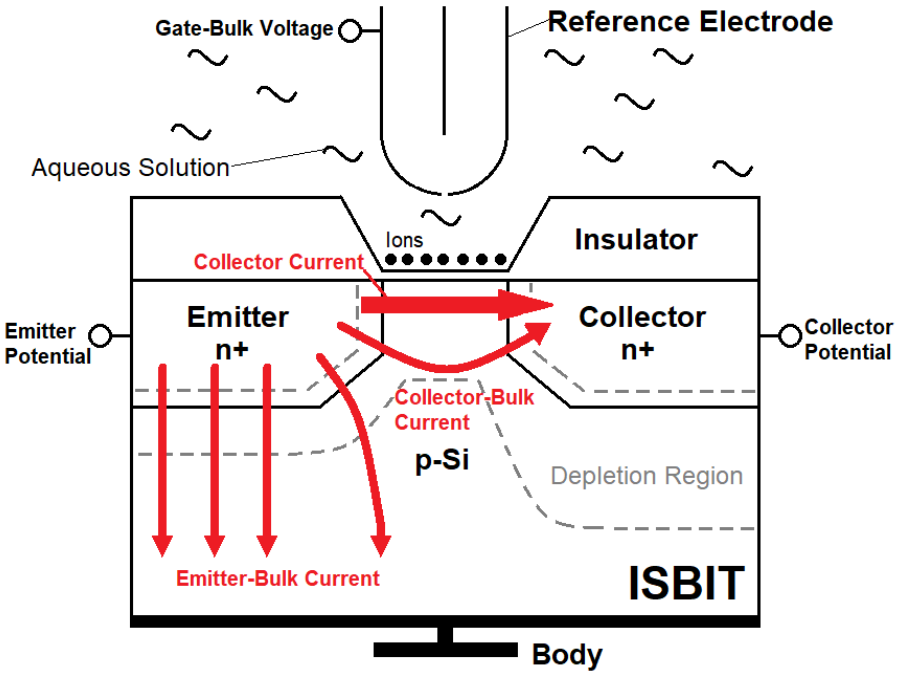

Figure 2.4: Cross-sectional view of an ISBIT.

Obviously, like in section 2.1, the currents and transconductances have to be defined in accordance with the new phenomena. The drain current, now becomes the collector current

$$I_C = I_{0C} \cdot e^{\frac{V_{GB}-V_{Th}}{\mu_T}} \cdot \left(e^{\frac{V_{BE}}{\mu_T}} - e^{\frac{V_{BC}}{\mu_T}}\right), \qquad [A] \tag{2.9}$$

with the additional emitter potential. [4] It already becomes apparent that the collector current is influenced by more indicators than the drain current in subthreshold. Notice the additional exponential within the brackets of equation (2.9), that isn't present in the parentheses of equation (2.1).

2.4 Derivation and Summary

To emphasize on the main difference and basically to deduce the correct superthreshold equations for the ISBIT a derivation is done for all three current and transconductance equations. Recall

$$I_C = I_{0C} \cdot e^{\frac{V_{GB}-V_{Th}}{\mu_T}} \cdot \left(e^{\frac{V_{BE}}{\mu_T}} - e^{\frac{V_{BC}}{\mu_T}}\right). \qquad [A] \tag{2.10}$$

Now, to get it to the same form as equation (2.1), the first exponential in the parentheses needs to come outside, which leads to:

$$I_C = I_{0C} \cdot e^{\frac{V_{GB}-(V_{Th}-V_{BE})}{\mu_T}} \cdot \left(1 - e^{-\frac{V_{CE}}{\mu_T}}\right) \qquad [A] \tag{2.11}$$

with $V_{BE} - V_{CE} = V_B - V_E - V_C + V_E = V_{BC}$. Equation (2.11) shows that the collector current of the ISBIT, is similar to the drain current of the ISFET plus an extra term for the voltage across the emitter and body. Substituting that additional V_{BE} term, the relations for linear and saturation collector current become:

$$I_C = \mu C_{Ox} \cdot (\frac{W}{L}) \cdot (V_{GB} - (V_{Th} - V_{BE}) - \frac{1}{2} \cdot V_{CE}) \cdot V_{CE} \qquad [A] \tag{2.12}$$

$$I_C = \frac{1}{2} \cdot \mu C_{Ox} \cdot (\frac{W}{L}) \cdot (V_{GB} - (V_{Th} - V_{BE}))^2 \qquad [A] \tag{2.13}$$

Even though V_{CE} is at hand in equation (2.12), it will not contribute to the collector current because it will be kept constant in the measurements to see pure characteristics and trends for the ISBIT. $V_{BE} = V_B - V_E$, however, will for both operating regions automatically increase the current given that the bulk voltage remains zero and the minus signs cancel out and so the emitter potential contributes positively. Equations (2.12) and (2.13) have the following effect on the transconductance in linear and saturation as

$$g_m = \frac{dI_C}{dV_{GB}}. \qquad [A/V] \tag{2.14}$$

When taking the derivative with respect to V_{GB} the eventual transconductances for the ISBIT become

$$g_m = \frac{I_{0C}}{m\mu_T} \cdot e^{\frac{V_{GB}-V_{Th}}{\mu_T}} \cdot \left(e^{\frac{V_{BE}}{\mu_T}} - e^{\frac{V_{BC}}{\mu_T}}\right)), \qquad [A/V] \tag{2.15}$$

$$g_m = \mu C_{Ox} \cdot (\frac{W}{L}) \cdot V_{CE}, \qquad [A/V] \tag{2.16}$$

and

$$g_m = \mu C_{Ox} \cdot (\frac{W}{L}) \cdot (V_{GB} - (V_{Th} - V_{BE})) \qquad [A/V] \tag{2.17}$$

for the subthreshold-, linear- and saturation operating region, respectively. Equation (2.15) shows that the transconductance in subthreshold will increase due to the bulk-emitter and the bulk-collector voltage. In the linear operating region, equation (2.16), g_m won't show any difference, because V_{CE} is equivalent to V_{DS} in equation (2.2) and is kept constant. But, in the saturation operating region, equation (2.17), again the bulk-emitter voltage will contribute to the transconductance. The complete current and transconductance model for the realized ISFET, hence with the corresponding parameters (more on this in Chapter 3), can be seen in figures 2.5, 2.6, 2.7 and 2.8.

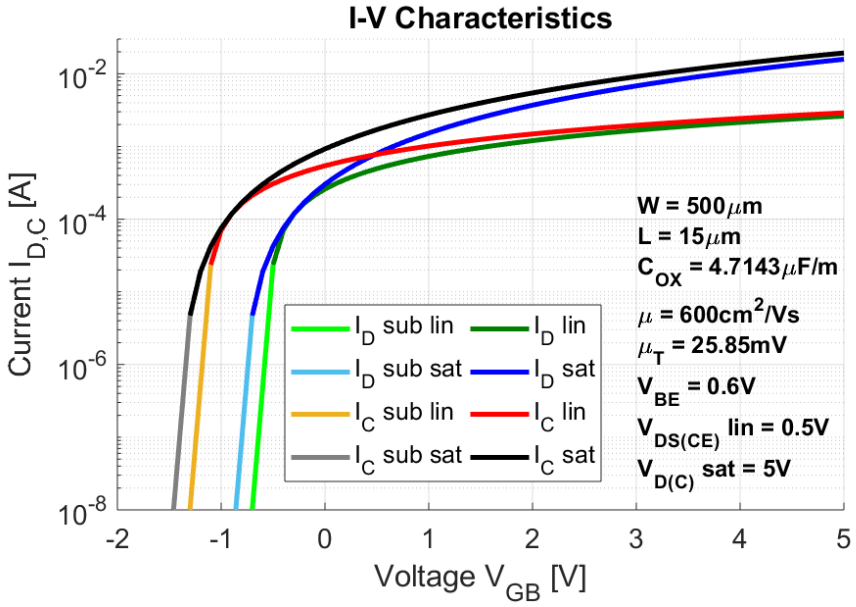

Figure 2.5: Current model (logarithmic) for the ISFET/ISBIT based on [7]

.

Figure 2.5 displays the current model on a logarithmic scale. In this particular scaling the subthreshold current just continuously increases not showing that the start value is one with 50 zeros in front, which would actually be a constant value here because it is so small. Anyways, the two linear curves are distinctively visible, as these, the red and green curve, converge to the same range. The saturation curves, blue and black, also converge to the same range and are comparatively higher than the linear current. Also, for both it becomes clear that the collector current is higher than the drain current in subthreshold. Additionally, the shift in threshold voltage by $0.6V$ is visible.

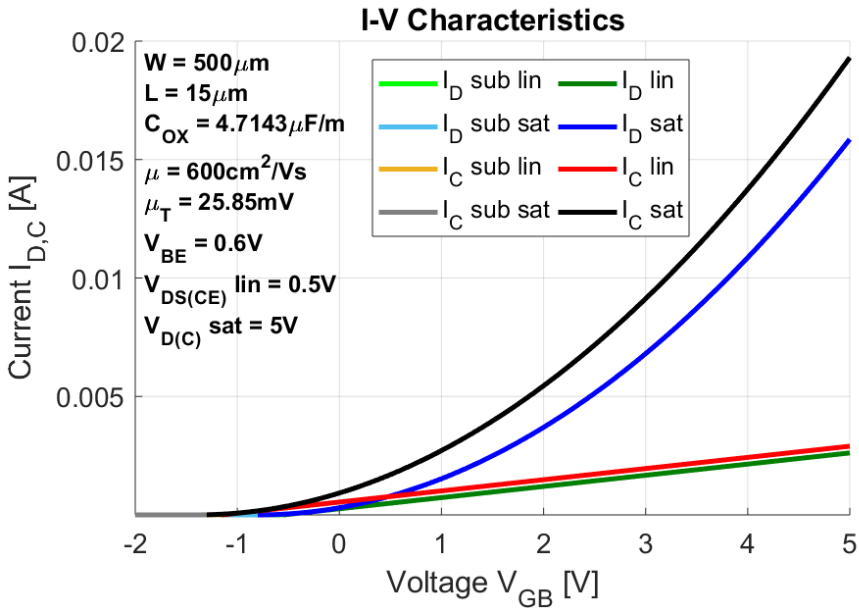

Figure 2.6: Current model (linear) for the ISFET/ISBIT based on [7]

.

In superthreshold the distinctions between the operating regions now becomes even more obvious as the saturation current increases quadratically and the linear current linearly. This can be seen in figure 2.6. Again, in both cases is the collector current of the ISBIT higher than the drain current of the ISFET.

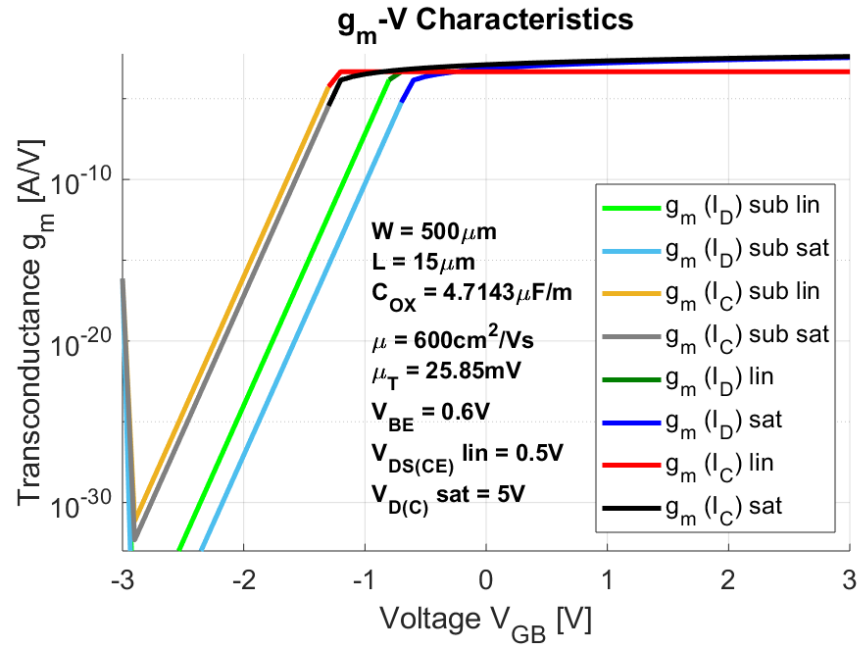

Figure 2.7: Transconductance model (logarithmic) for the ISFET/ISBIT.

The transconductance in correspondence with the previous collector and drain current can be seen in figure 2.7. In subthreshold it becomes apparent that again g_m is higher for the ISBIT in comparison with the ISFET.

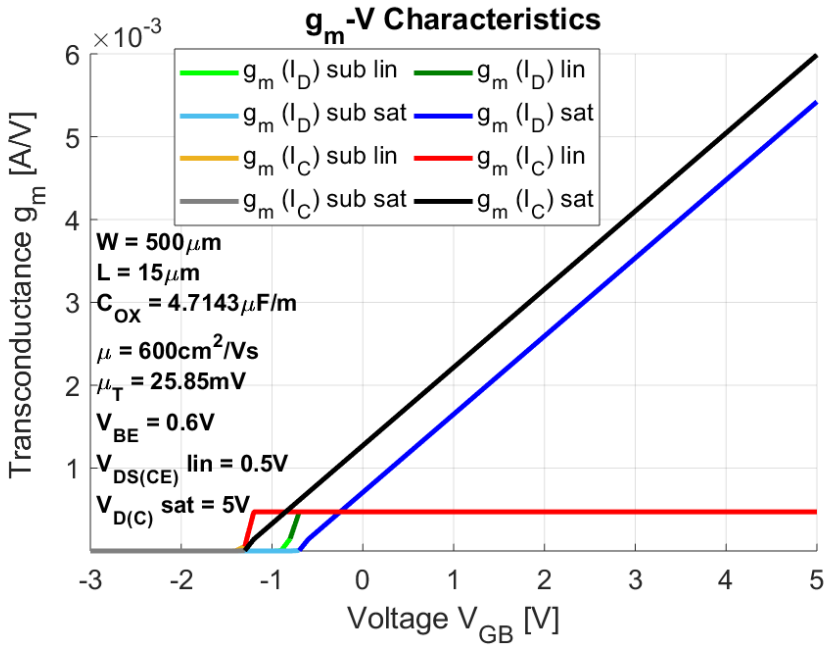

Figure 2.8: Transconductance model (linear) for the ISFET/ISBIT.

On a linear scale, figure 2.8, only the superthreshold transconductance in the saturation operating region is higher for the ISBIT. It can be described as a linear increase. The g_m in the linear operating region appears to be a constant value and doesn't show any difference between the two with the exception of a shift in threshold voltage, again by $0.6V$.

It becomes apparent through comparing equations (2.1), (2.2) and (2.3) with (2.9), (2.12) and (2.13) and examining figures 2.5 and 2.6, that the current in all three operating regions will increase. In the superthreshold graph, the improvement is clearly visible for linear and saturation, which is caused by the V_{BE} term. In subthreshold the current becomes considerably higher because of again the bulk-collector exponential within the parentheses. A shift in the threshold voltage is visible and anew caused by V_{BE}. Now, in regards to g_m this term can only be found in the subthreshold and saturation transconductance. Indicating, that it will only increase in these two operating regions and in fact not in the linear one (equations (2.5), (2.6), (2.7), (2.15), (2.16) and (2.17), also figures 2.7 and 2.8). In order to see trends for each pH values, recall equation (2.8), which can be substituted in each equation to accommodate for the variables. It is expected that a variation will be noticed on the basis of the pH value as far as current and transconductance are concerned, because V_{GB} is now a function of the pH value.

Chapter 3

TCAD Simulations

In this chapter, the two dimensional Technology Computer-Aided Design, abbreviated TCAD, simulations are discussed for the drain and collector current and their corresponding transconductances of both the ISFET and ISBIT in the linear and saturation operating region. In fact, these simulations were performed with the specific ISFET configuration as used in the actual experiment. After the simulation results are shown a short description followed by a short interpretation is given. Next, a small section discussing the occurrences is provided. Side-note, because the simulations are performed in two dimensions, the unit of the current becomes $[\frac{A}{\mu m}]$ and the unit of g_m becomes $[\frac{A}{V\mu m}]$.

3.1 The practical ISFET

A top view layout of the ISFET is shown in figure 3.1 and a side view in figure 3.2. Both figures show the dimensions. They also provide a better overview of how the terminals are arranged. The gate-oxide surface only consists of $120nm$ of the pH sensitive Ditantalum-Pentoxide or in short Tantalum Oxide (Ta_2O_5), as being the oxide with direct contact to the aqueous solution, and an additonal $70nm$ of Silicon-Dioxide (SiO_2). The gate length is $15\mu m$ and the gate width is $500\mu m$. Ta_2O_5 is used because it has the largest buffer capacity out of the usual oxides. A very large buffer capacity of a surface is the equivalent of providing a constant surface ion concentration that is independent to fluctuations in pH and ion concentration, and hence, Ta_2O_5 is the best oxide to donate or accept ions. [3] While figure 3.1 is better to get an overall view of the location and size of each component, figure 3.2 is more useful regarding the complete allocation and layering within the device. The n-type ISFET has a boron p-doped Si substrate with integrated boron stopper diffusion, where the substrate is in contact with the oxide layering except at the gate, and with the n-doped phosphorous source and drain terminals. The aluminum

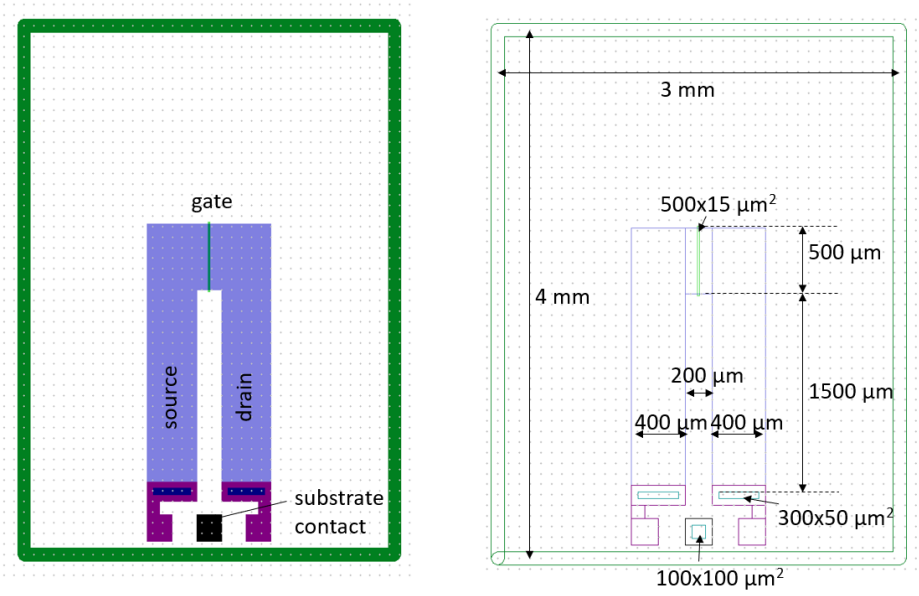

Figure 3.1: Schematic top-view of the realized ISFET with dimensions and labeling [5]

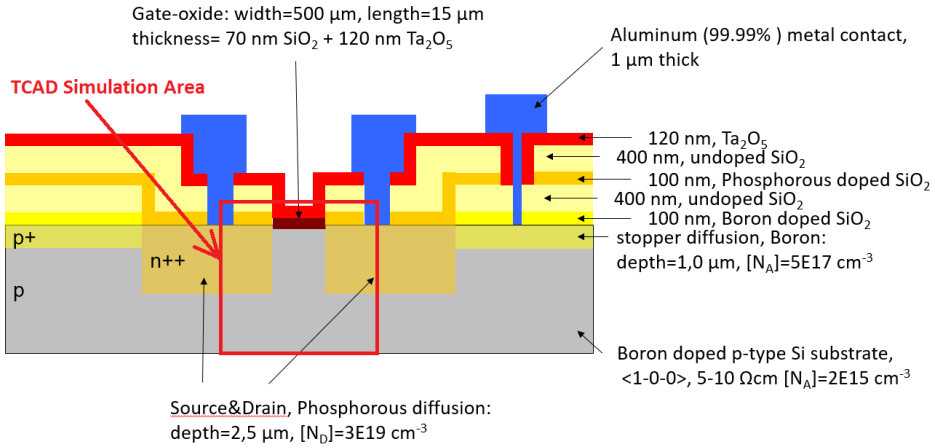

Figure 3.2: Schematic cross-section of the realized ISFET with indicated simulation area, aimensions and labeling [5]

contacts reach all the way down to their respective terminals (source, drain and also body). Besides the gate consisting of SiO_2 and Ta_2O_5, the layering in the rest of the device also features $100nm$ boron doped Si underneath- and $100nm$ of phosphorous doped Si in between two layers of $400nm$ thick undoped Si. Figure 3.2, additionally, indicates the area where the TCAD simulations were performed.

3.2 Linear Operating Region

In figure 3.3 and 3.4, the current and the transconductance are plotted based on the TCAD simulations. Specifically, these are the results in regards to the linear operating region of the ISFET/ISBIT. The following settings for the ISFET simulations were applied. The source and the body both had a bias voltage of $0V$. The drain, however, was supplied with a constant $0.6V$, while the gate was swept from $-2V$ to $+2V$. To obtain the ISBIT simulation results, the zero bias is now applied on the collector. For a good comparison V_{DS} or rather V_{CE} is fixed. Additionally, the emitter now has $-0.6V$ as bias voltage and the gate sweep remains the same as before. [5]

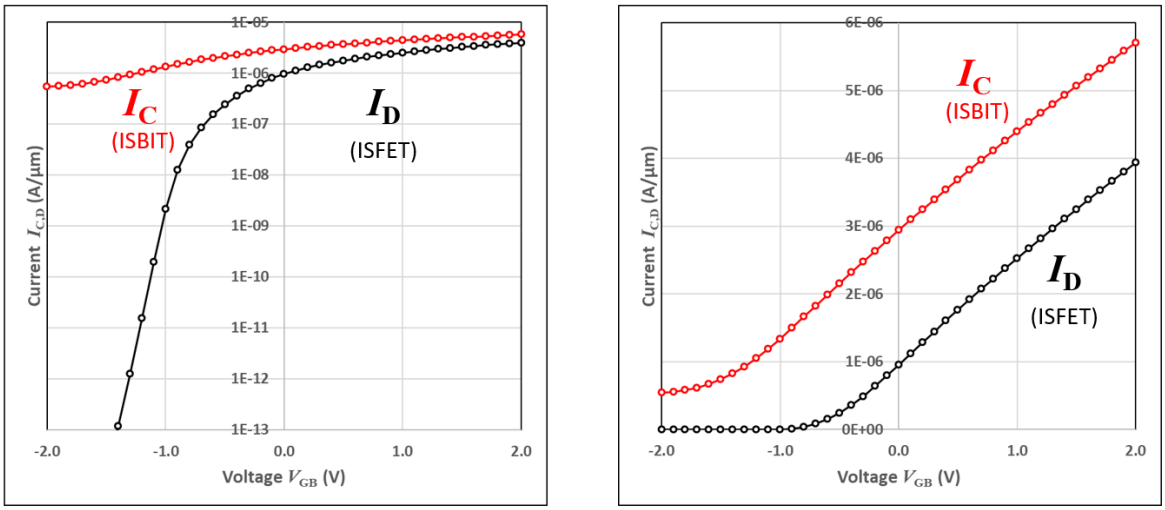

Figure 3.3: $I_{D,C}$ in linear operating region. [5]

Figure 3.3 shows the current on a linear (right) and on a logarithmic (left) scale. At first, a description is given for both, starting with the left figure. For approximately $V_{GB} = -1.5V$ the drain current has a very sharp increase. This continues until $V_{GB} = -0.8V$ when the slope starts to decrease again. The collector current, however, shows a higher constant current level, much higher than the drain current. After about $V_{GB} = -1V$, this graph also converges to the $10^{-6}\frac{A}{V\mu m}$ range. Beyond this point, the properties can better be analyzed with the linear scale on the right. Here, the drain current starts increasing linearly roughly after $-0.9V$, while the collector current already starts doing that at about $-1.6V$. Noticeably, the collector current also has a higher starting value on this scale, just as before on a logarithmic scale.

The substantially higher subthreshold current can be traced back to the collector-bulk current flowing underneath the channel region (eq. (2.9)). In superthreshold the collector current is higher than the drain current due to the V_{BE} term. The shift of collector current is the threshold voltage shifting due to the supplied emitter potential. When comparing both of these figure with 2.5 and 2.6, it becomes obvious that the model is very accurate. The only thing that stands out is the leakage in collector current in subthreshold present in the left graph of figure 3.3.

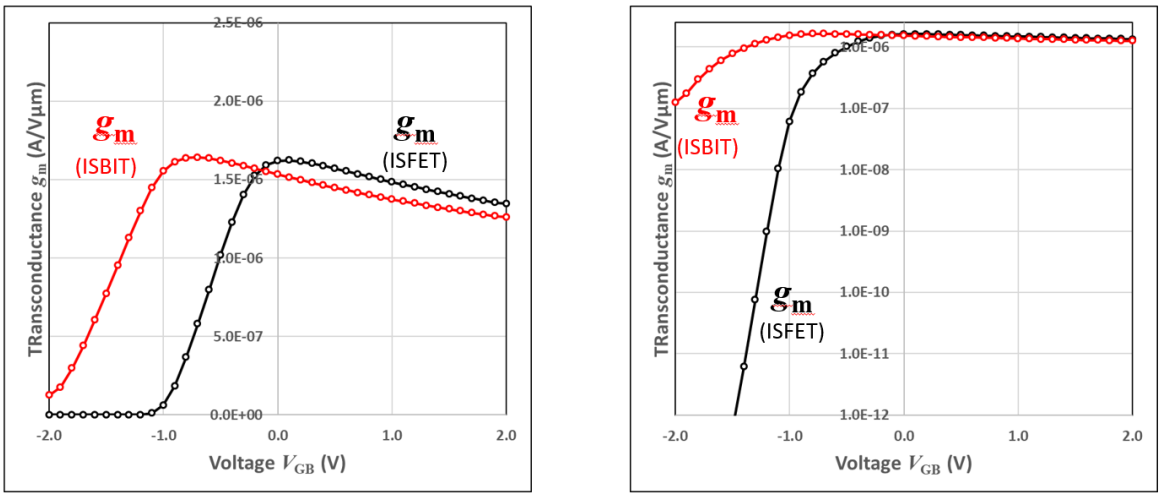

Figure 3.4: g_m in linear operating region. [5]

The transconductances, figure 3.4, that are based on the previous current graphs are now described. On a logarithmic scale, which is on the right hand side, the transconductance of the ISFET increases from $V_{GB} = -1.5V$ to round about $V_{GB} = -0.5V$. After that it is followed by a decrease which ever so slightly noticeable. Anew, the ISBITs' g_m has higher values and increases from $V_{GB} = -2V$ to $V_{GB} = -1V$. It can be seen that it also decreases slightly, beyond that point. On the left side, the same graphs are scaled linearly. For the ISFET the graph ramps up after passing the threshold voltage at $V_{GB} \approx -0.8V$. A stronger decline can now be observed after $V_{GB} \approx -1.5V$. The ISBITs' transconductance is very much the same in terms of the course of the graph, only it appears to be shifted by approximately $-0.9V$.

On the logarithmic scale, the subthreshold transconductance for the ISBIT can be seen to be substantially higher than the g_m of the ISFET, due to the same reason as previously for the collector current. The collector-bulk term provokes an additional contribution to the current and consequentially also the transconductance, as can be seen in equation (2.9) and (2.15). With the exception of the shifted threshold, which is caused by the emitter potential, both g_m curves are the same in the linear operating range, not completely confirming equation (2.6) and (2.16). In fact, after reaching their local maximum the decline followed by that can be explained with the

fact that the charge carriers are pulled against the oxide by the electric field reducing their mobility. The subthreshold transconductance was modelled very well in figure 2.7. But, in superthreshold the transconductance, here, isn't a constant value. Quite the contrary, actually, as described above.

So, already in the simulations it is somewhat confirmed what was expected in section 2.3. The subthreshold current and transconductance are higher in the ISBIT than in the ISFET and so is the linear collector current in superthreshold. However, in this operating region the transconductance in superthreshold only shows improvement near the threshold voltage. After surpassing the maximum transconductance there is a even a decrease in g_m noticeable in comparison from ISBIT to ISFET, which wasn't as expected in the model nor in the whole theory section.

3.3 Saturation Operating Region

In the following TCAD saturation simulations the drain (collector) potential on both ISFET and ISBIT was set to $5V$. Nevertheless, for the ISFET the source had a bias voltage of $0V$ and the ISBITs' emitter was supplied with $-0.6V$. The gate-bulk voltage is now swept from $-2V$ to $5V$.

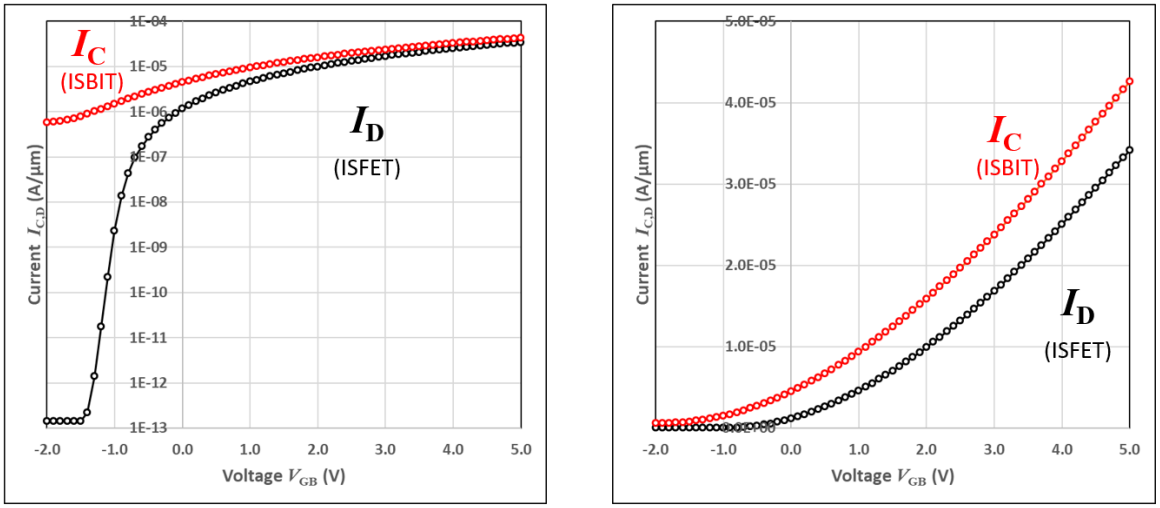

Figure 3.5: $I_{D,C}$ in saturation operating region. [5]

What can be seen on a logarithmic scale, in the left graph of figure 3.5, is that the drain current starts to be influenced by the gate-bulk voltage at around $V_{GB} = -1.5V$. After that the current increases until its slope becomes less steep after $V_{GB} \approx -0.5V$. For the collector current that already has significantly higher subthreshold values, the gate-bulk voltage starts influencing it after $V_{GB} = -1.7V$. Scaled linearly, both the drain and collector current now increase quadratically after the threshold voltage is surpassed. One more time, the collector current achieves slightly higher values and appears to be shifted by $\approx 1V$.

In subthreshold the same thing applies here just like in the simulation of the linear current and transconductance. It is significantly higher, due to the collector-bulk current. In superthreshold, the collector current is higher because of the bulk emitter voltage, can be seen in equations (2.9) and (2.13). The shifted threshold can again be based on the same fact. Comparing this figure with the model, shows that again for the current the theory model is very accurate. One thing that wasn't accommodated for is the leakage current for the ISBIT in subthreshold.

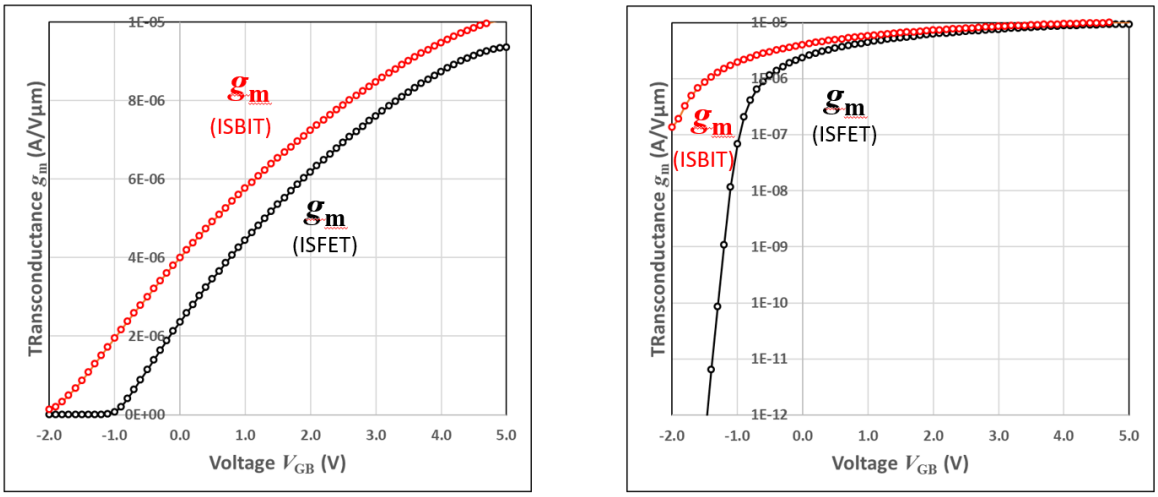

Figure 3.6: g_m in saturation operating region. [5]

In figure 3.6, both transconductances in the saturation operating region are displayed. In the logarithmic scaled case, which is on the right, g_m of the ISFET increases with a very steep slope after $V_{GB} = -1.5V$. After that, the transconductances converge to the $10^{-6}\frac{A}{V\mu m}$ range. The transconductance of the ISBIT has an increase visible from $V_{GB} = -2V$ to approximately $V_{GB} = -1V$. On a linear scale, g_m of the ISFET reaches threshold around $V_{GB} = -1V$ and starts rising to its local maximum in the figure. The ISBITs' transconductance reaches threshold earlier ($V_{GB} = -1.9V$) and then also increases over the whole span of the gate-bulk voltage. Again, g_m of the ISBIT appears to be shifted by $0.9V$ and with that achieves higher overall values.

While subthreshold transconductance and threshold voltage shift are caused by the same reasons as previously, the saturation transconductance is higher because of the V_{BE} term, as can be seen in equation (2.17).

Hence, in the saturation operating region, the sub- as well as the superthreshold collector current and transconductance are higher in the configuration of the ISBIT. This is as expected in section 2.3 and additionally the current model, figures 2.5 and 2.6, for both sub- and superthreshold was confirmed. With exception of the leakage current that is visible in the simulations (figures 3.3 and 3.5), but not in the current model. The transconductance model was only partially confirmed as well, because the decline in slope isn't taken into account.

Chapter 4

Experimental

Disclosed below are the set-ups and a protocol for each performed measurement. It includes the measurement equipment, the environment, the approach and so forth. Initially, the reference measurements, which were basically done in a ”dry” environment, of the MOSFET and MOSBIT were performed. This is followed by the measurement of ISFET and ISBIT. The chapter ends with a detailed summary of each measurement procedure.

4.1 MOSFET and MOSBIT Measurement Set-Up

All measurements were performed with the same equipment, to be specific, the Keithley 4200-SCS. It is a device especially useful for analyzing of the DC characteristics of semiconductors. While its multiple incoming and outgoing channels can be attached in various combinations, the four force and sense channels were used during the reference on-wafer measurements combined with a probe station. The data was processed with the help of the installed KITE software, in a way that this software allowed to force a voltage upon the transistors via the force connections and then ultimately any parameter could be sensed with the sense channel.

Regarding the MOSFET and MOSBIT reference measurements a constellation of Keithley, probe station and wafer was set up. This wafer had a total of three MOSFETs glued to it. These MOSFETs are more or less identical to the ISFETs, with obviously a normal gate terminal, as they were fabricated in the same process. The wafer was placed on top of the chuck of the probe station. With the help of the base rough positioning of the transistors was possible. Not only could this section move back and forth, horizontally and vertically, but it also produced a vacuum beneath the wafer to keep it in position at all times. After raising the wafer into a suitable height, the actual electric probes had to be maneuvered towards the terminals. In this phase everything had to be done through a microscope. The probes could also

be moved back and forth as well as left and right, but upon reaching the desired terminal, the probe had to be moved downwards to establish a connection from the device to the Keithley system. Now, the only thing left was to ensure no influence of light, sound or temperature variations. This requirement could be fulfilled with the metal shielding that surrounded the probe station. These metal shields are in the form of two hatches, which could simply be shut with a locking mechanism and one cover that could be completely removed from the probe station.

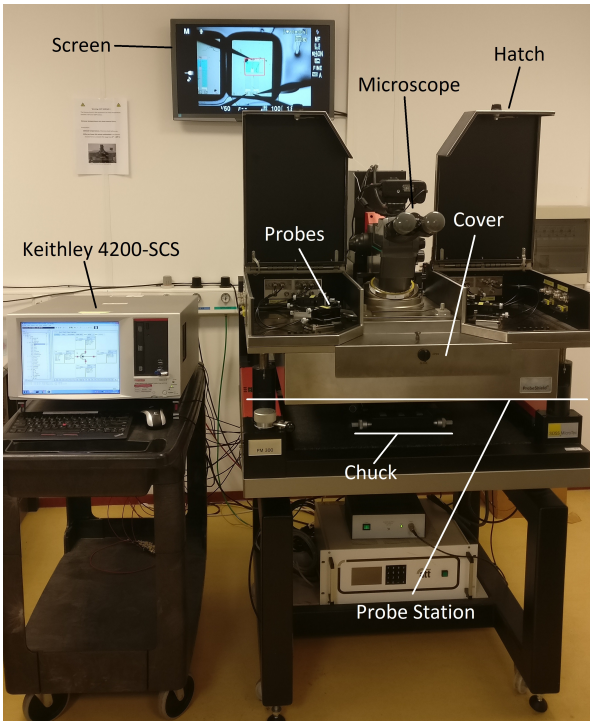

Figure 4.1: The used probe station with the Keithley SCS system.

4.2 ISFET and ISBIT Measurement Set-Up

To guarantee no influence of the outside world was tougher to accomplish while performing the ISFET and ISBIT measurements. The underlying reasons are formed by the technique with which ISFETs were measured. These transistors had to be submerged into an aqueous solution together with a reference electrode. Anyhow, the plastic container including all of the above has to have a specific reference electrode and the ISFET in contact with the triax connectors of the Keithley, while the surroundings should still not affect the semiconductor devices. This forced the manufacturing of a suitable casing that fulfills these requirements. A simple square-shaped box was used which only needed the triax connectors screwed on top of it and isolation on the opening (a small door) to make it impenetrable by light. Inside, all conducting

parts needed a wire soldered to it, for the actual connection and also for possible later use with different connections. So, a case was created that assured enough space for the plastic container, including the reference electrode, the ISFET and the solution, an established connection with the Keithley and minimal influence from the outside world. A sketch is depicted in figure 4.2. This box only has four connectors, so only four cables of the Keithley could be attached. Hence, only the force connections were used for these measurements. This might cause a deviation in the measurements, so one MOSFET measurement had to be repeated without the sense connections to see whether this is actually possible and if so, how significant this variation is. It was determined that it only altered by about a factor of $10^{-15}A$ in the specific measurement. So, there was no significant difference. Additionally, the integrated wires didn't cause any oscillation, which might have been possible, because the Keithley actually works with precisely measured cables. Another factor that could have been a source for disturbing the results, are the different pH values that are used during the measurement. Here, the pH values were 4, 7 and 10.01, representing relatively acidic, neutral and relatively basic, and implies a great difference in the number of ions present. Therefore, after every round of measurements with the ISFET, and in fact the reference electrode too, had to be deionized with the aid of either deionized, demineralized or distilled water.

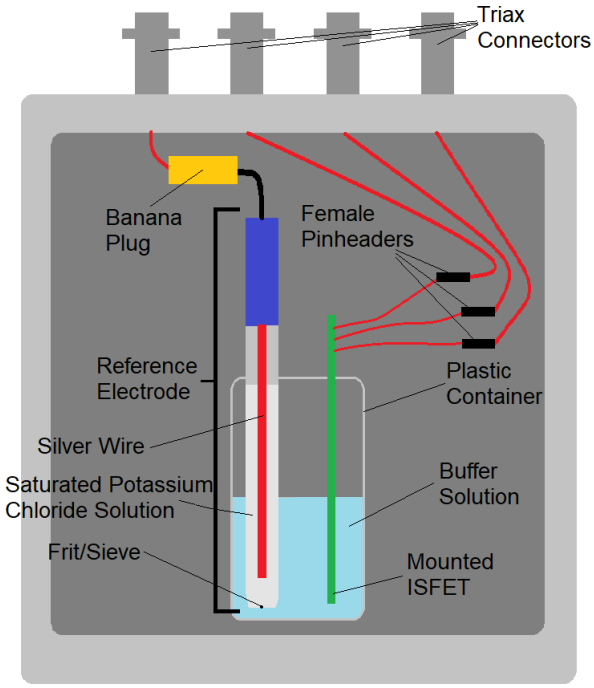

Figure 4.2: Rough drawing of ISFET measurement set-up.

4.3 Measurement Protocol

The location of the experiment was the laboratory of the IDS group in the Carré building on the campus of the University of Twente. Specifically, in a Faraday cage, but the door was always open. Not only were the measurements performed in the same location with the exact same devices and equipment but also the temperature, sound level and lighting were kept intuitively the same.

4.3.1 Reference Measurements (MOSFET/MOSBIT)

At first, the wafer was taken out of its casing with a wafer pincer and carefully placed on the chuck of the probe station. The vacuum system of the probe station to keep the transistors in position was then switched on. The next step was to roughly position the wafer, as this bottom section is free to move in all directions, when locked out of position by pressing the corresponding buttons. Otherwise, it remains fixed at all times. When this positioning was completed the height was adjusted and the right lens for the microscope had to be chosen to get a clear view of the devices and probes. The monitoring of this very small area was done with a camera that would project it onto a screen above the probe station. However, for this also a light source was needed. Now, before the probes could be adjusted, the wafer had to be raised once more with another lever, bringing it to its final height. Then, each probe was maneuvered to one of the terminals. For the MOSFET/MOSBIT measurements SMU 1 was connected to the bulk, SMU 2 to the drain. SMU 3 to the gate and SMU 4 to the source terminal. A probe making clear contact with a terminal could be determined by recognizing a shift of the needles. This meant that the needle couldn't move any further downwards and hence moved in the direction of the least mechanical resistance. This connection had to be ensured for all terminals or else the measurements simply wouldn't work. Before actually measuring, the camera and the light had to be turned off, the mentioned (section 4.1) hatches had be closed and the cover had to be placed back into position. So, finally in the KITE software the corresponding SMU assignments were made and the settings were applied for each measurement. Since, there were three MOSFETs the order of measuring mostly was from left to right. Left and right was orientated with the help of the flat edge of the wafer. After the MOSFET, the MOSBIT measurements were performed. However, not always did the measurements go smoothly. Some had to be repeated and some new measurements had to be added as well. So, generally speaking, there were multiple round of measurements.

4.3.2 ISFET/ISBIT Measurements

In section 4.2, a custom made square-shaped box was described. The first step was to find a stable surface to place this box on. After that, the covers were removed from the triax connectors such that the force cables of the Keithley system could be attached. Now, once the box was in position, the content had to be assembled. A start was made by connecting the reference electrode via a banana plug. Before inserting the reference electrode and the mounted ISFET into the particular buffer, which was contained in a small plastic bottle, both had to be cleaned. This was to prevent any influence of unwanted ions that might have been present on both. This cleaning was done with the aforementioned demineralized water. Again, after every completed measurement with an ISFET or a buffer, all components in contact with the buffer, were deionized. On the mounted ISFET the wires had to be soldered onto very small contacts, making it very fragile. So, the ISFET was connected very carefully to the internal wires of the casing via female pin headers. Finally, it was made sure that there was no incident light in the box, before it was closed. Then, in the KITE software the connections were assigned. This time, SMU 1 was connected to the drain, SMU 2 to the gate, SMU 3 to the bulk and finally SMU 4 to the source. This turned out to be the most convenient with the internal wiring of the box itself and the mounted ISFET. The measurement order was both ISFETs after one another for one buffer solution, then to measure the ISBIT and then switching the buffer.

Chapter 5

Results and Discussion

In this chapter, the results of the ISFET and ISBIT measurements are displayed. For every figure a description andits interpretation is provided. Both of these will focus on the general course of the curves and the main difference between the two devices. If something particular stands out, it will be mentioned separately. Additionally, the corresponding measurement settings are listed in a table. At first, the ISFET/ISBIT results are presented for both the linear and saturation operating region. To be specific, the current and transconductance curves are shown on a linear and on a logarithmic scale. However, for these measurements a separate distinction for each pH value is made, showing the trends and characteristics of the ISFET and ISBIT in correspondence with the pH value. After each of these subsections a discussion summarizes the observations. The dry, or rather, the MOSFET/MOSBIT measurement results can be seen in appendix A. In the end, the MOSFET/MOSBIT measurements showed exactly the same outcomes as far as current and transconductance are concerned.

5.1 ISFET and ISBIT Measurements

The results shown below are in the linear and saturation operating region for the buffer with $pH = 4$ and only for one of the two provided ISFETs. The remaining results for $pH = 7$, $pH = 10.01$ and the other ISFET are displayed in appendix B.

5.1.1 Linear Operating Region

Table 5.1: Settings for the Step Measurement in Linear

Device Terminal	Instrument	Forcing Function	Start/Level [V]	Stop [V]	Step [V]
Drain	SMU1	Voltage Step	0.5	-0.3	-0.2
Gate	SMU2	Voltage Sweep	-3	5	0.1
Bulk	SMU3	Voltage Bias	0	N/A	N/A
Source	SMU4	Voltage Step	0	-0.7	-0.2

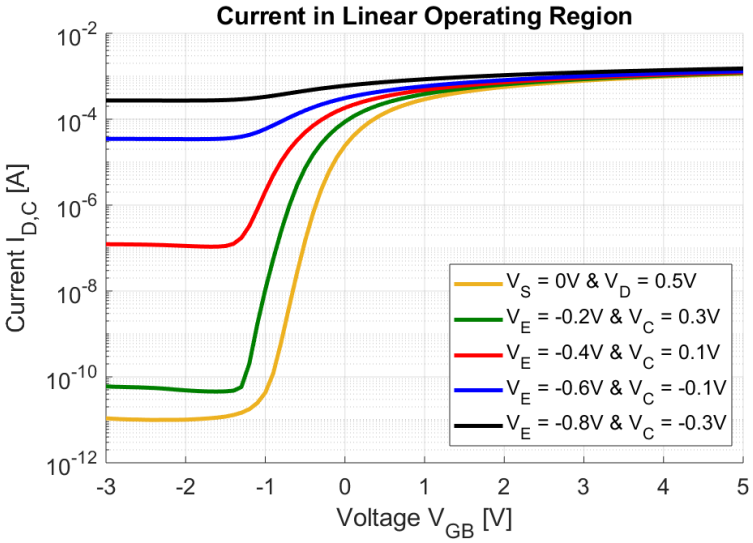

Figure 5.1: ISBIT measurement in linear operating region logarithmic scale.

Figure 5.1, displays the drain and collector current over the gate-bulk voltage on a logarithmic scale for a fixed $V_{CE} = V_{DS} = 0.5V$. Each curve appears with a very low constant value. After a specific value for the gate-bulk voltage, the curves starts increasing until reaching the threshold voltage. Beyond that point, characteristics can better be analyzed on a linear scale. The slope of the increase towards the threshold voltage decreases every time, because the start value becomes higher each time.

Each time when V_E is decreased, the subthreshold current increases significantly. This is caused by the collector-bulk current, equation (2.9). The difference between the yellow drain current and the black collector current is in the range of $10^7 A$. Also, it seems that the threshold voltage is shifted for a more negative emitter potential.

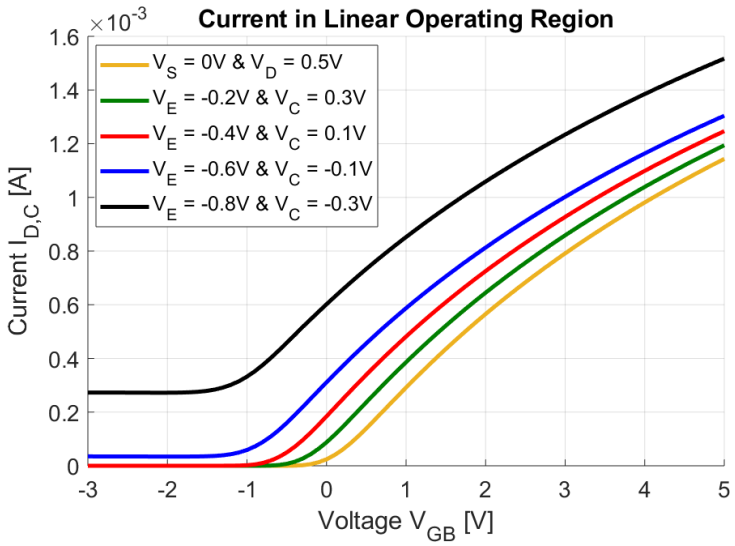

Figure 5.2: ISBIT measurement in linear operating region.

Now, figure 5.2 shows the same currents on a linear scale. Each graph starts increasing linearly after reaching its corresponding threshold voltage. This linear increase has the highest steepness right after initiating and decreases slightly in slope the higher V_{GB} becomes. The collector current with $V_E = -0.7$ and $V_C = -0.3V$ shows a dramatic increase as it is so much higher than the previous blue curve, about $0.2 \cdot 10^{-3}A$.

This time in superthreshold, the increase in current every time V_E is decreased can be reasoned with the V_{BE} term contributing to the collector current, equation (2.12). The negative V_E cancels out the minus sign, which makes the whole term positive and hence increases I_C. Hence, the collector current provokes an increase in sub- as well as in superthreshold. Again, the shift in threshold voltage is the V_{BE} term.

Transconductance Linear

On a logarithmic scale, the transconductances in the linear operating region, figure 5.3, fluctuate strongly in subthreshold. The transconductances increase sharply after a certain V_{GB} is reached and eventually converge to the $10^{-4}A/V$ range.

Ignoring the noise and focusing on the exponential increase towards the threshold voltage, it can still be seen that the collector current increases every time V_E decreases. This increase is caused by the collector-bulk component, equation 2.15.

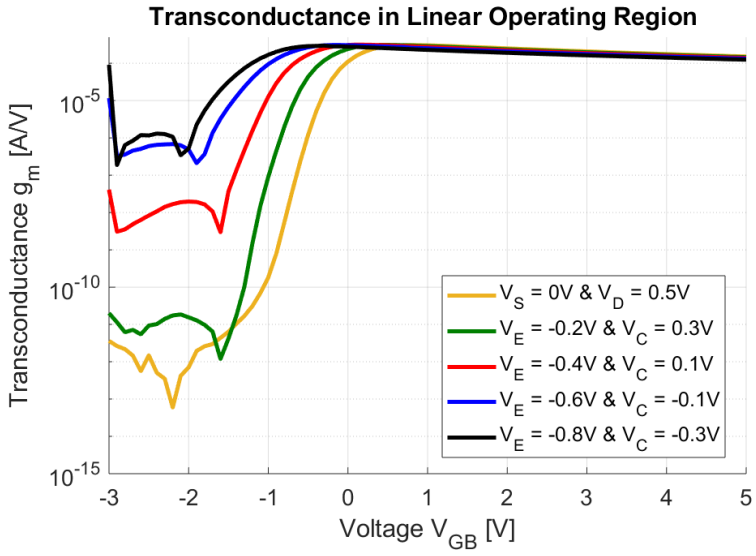

Figure 5.3: ISBIT measurement transconductance in linear operating region logarithmic scale.

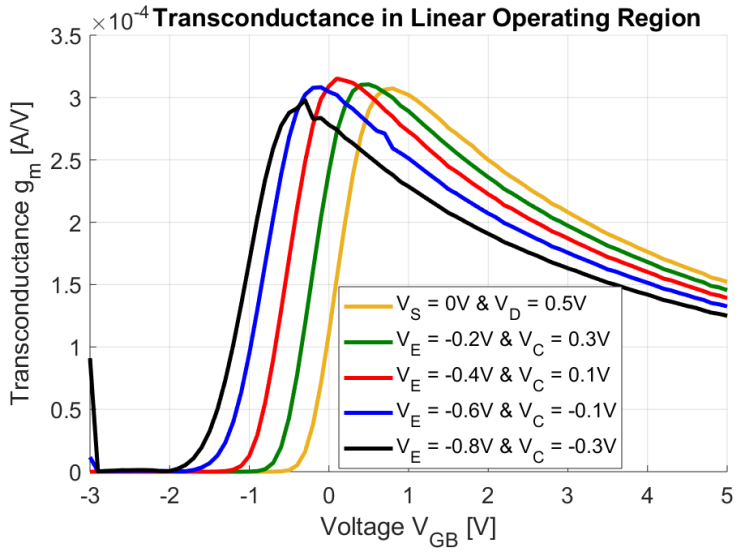

Figure 5.4: ISBIT measurement transconductance in linear operating region.

In figure 5.4 the same transconductance can be seen on a linear scale. After reaching threshold, the transconductances start increasing to their respective local maximum. If that specific point is reached, each curve decreases again and all of them seem to converge to the same value, approximately.

Generally, the transconductances only seems to improve near the threshold voltage. The red collector current with $V_E = -0.4$ and $V_C = 0.1V$ appears to have the maximum transconductance although it is really only minimally higher than the rest. This indicates that there might be a slim optimum. Anyhow, the shift in threshold volt-

age can still be observed, which is again caused by the supplied emitter potential. Furthermore, each g_m decreases after reaching the local maximum. This can be traced back to a mobility reduction of the charge carriers, as the electric field pulls the charge carriers against the silicon surface slowing them down. But, even more important the transconductance reduces from ISBIT to ISFET after surpassing this local maximum.

So, in the linear operating region both the current and the transconductance increase in subthreshold. However, in superthreshold only the current increases over the whole span of V_{GB}, the transconductance only does so near the threshold voltage. And, after reaching their local maximum a decrease for the transconductance can be seen. This not completely as expected in chapters 2 and 3. The current model is generally a good representation. But, the transconductance model indicated that g_m would be a constant value, which is not the case in practice, in a sense that it increases to a maximum and then decreases because of the mobility reduction of the charge carriers in superthreshold. However, the simulations already pointed both of these factors out and, hence, correspond with the measurements.

5.1.2 Saturation Operating Region

Table 5.2: Settings for the Step Measurement in saturation

Device Terminal	Instrument	Forcing Function	Start/Level [V]	Stop [V]	Step [V]
Drain	SMU1	Voltage Bias	5	N/A	N/A
Gate	SMU2	Voltage Sweep	-3	5	0.1
Bulk	SMU3	Voltage Bias	0	N/A	N/A
Source	SMU4	Voltage Step	0	-0.7	-0.2

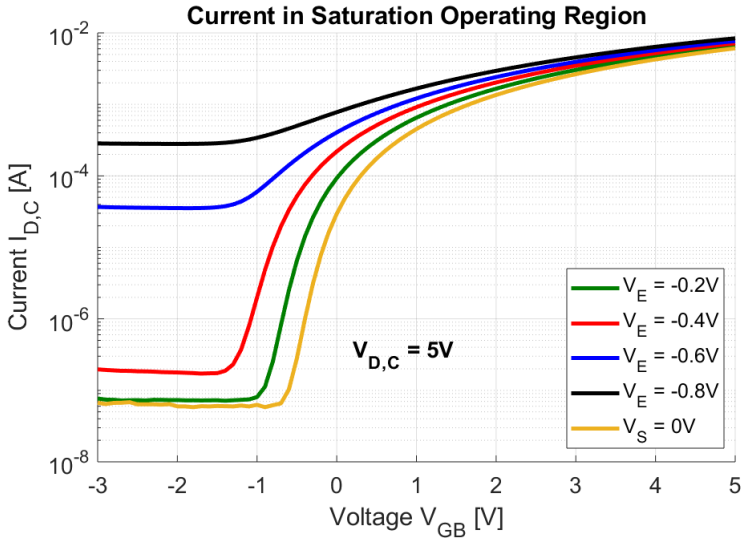

Figure 5.5: ISBIT measurement in saturation operating region logarithmic scale.

The current in the saturation operating region on a logarithmic scale for a fixed $V_D = V_C$ can be seen in figure 5.5. Again, the course of all curves starts with a very small constant value. A steep increase after a particular instance on V_{GB} can be seen. Finally, after the threshold voltage is reached the curves converge to a range for which it is better to analyze the current on a linear scale. The start value becomes higher each time. Also, a shift can be observed.

Refer to equation (2.9) to see that once more the exponential term for the emitter- and collector bulk currents influence this subthreshold current severely. The jump from I_D to I_C, with $V_E = -0.2V$ and $V_C = 0.3$, isn't too significant, but it is the only instance not showing a major increase. The shift in threshold voltage, anew, is cause by the V_{BE} term in equation (2.13).

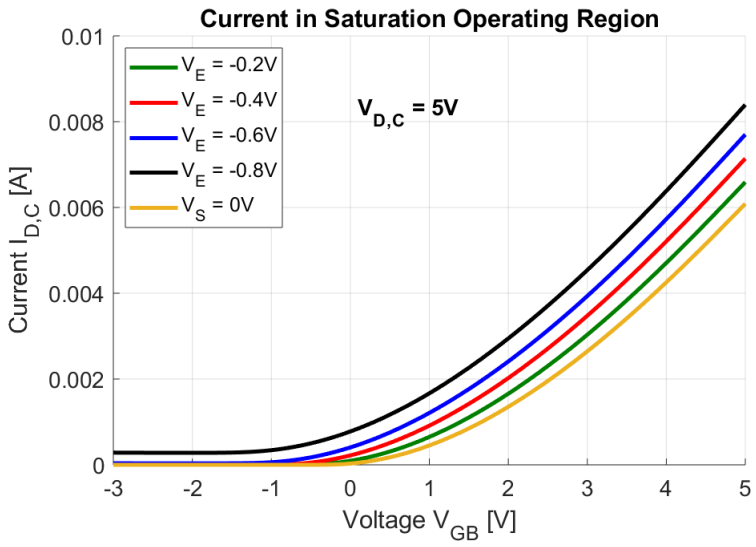

Figure 5.6: ISBIT measurement in saturation operating region.

Figure 5.6 shows the drain and collector currents over the gate-bulk voltage in the saturation operating region and on a linear scale. All curves have the quadratic increase after their respective threshold voltage is reached. Another slight shift of the complete graph can be seen each time.

The higher values for each collector current can be traced back to the V_{BE} term in equation 2.13. which now even quadratically contributes to the current. The emitter potential also shifts the threshold voltage.

Transconductance Saturation

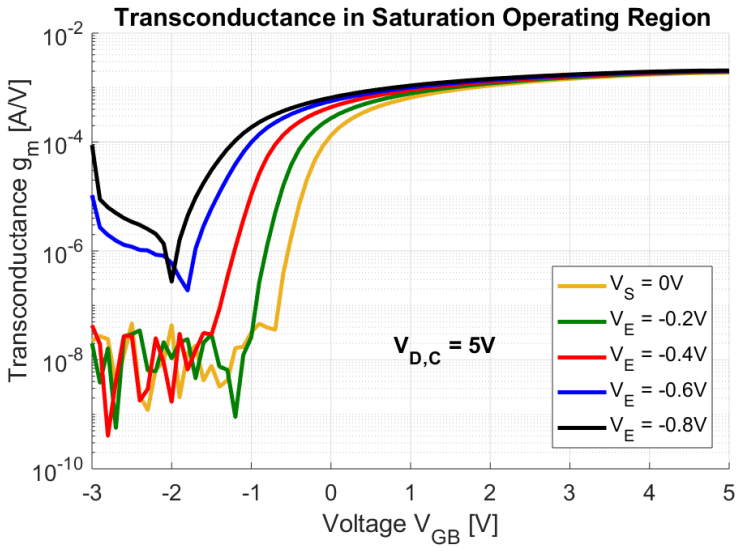

Figure 5.7: ISBIT measurement transconductance in saturation operating region logarithmic scale.

The logarithmically scaled transconductances in the saturation operating region can be observed in figure 5.7. This time the fluctuations in subthreshold are more frequent and more intense than previously in figure 5.3. However, the initial point on V_{GB} that is followed by an increase to the threshold voltage is still noticeable.

These fluctuations again are simply noise. An increase in subthreshold transconductance for every time the emitter potential is decreased becomes obvious during the exponential increase for all transconductances. Once more is this increase caused by the collector bulk component (eq.(2.15)).

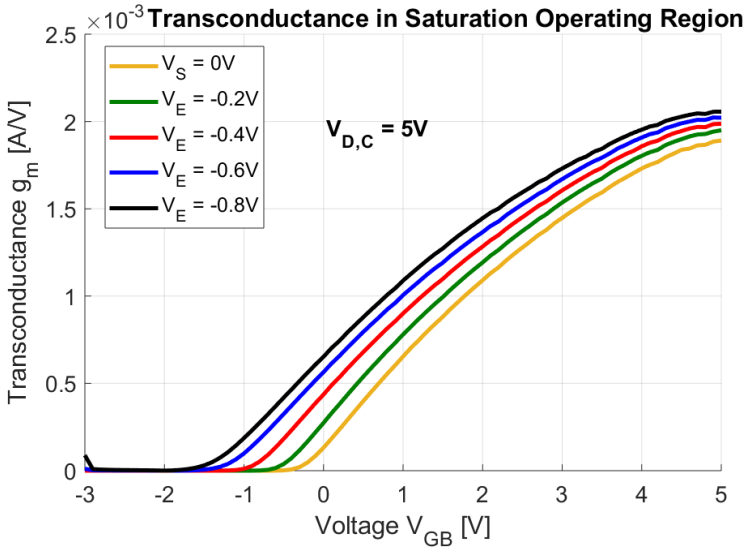

Figure 5.8: ISBIT measurement transconductance in saturation operating region.

In figure 5.4, the same transconductances are plotted on a linear scale. All curves increase after reaching the threshold voltage and start to rise towards their local maximum. Each time V_E is decreased a shift to the left is noticed.

The transconductances in superthreshold for the saturation operating region increase because of the bulk-emitter voltage term as can be seen in equation (2.17). Once more, the shift in threshold voltage is also caused by this voltage.

In the saturation operating region, the current and transconductance are higher in the ISBIT than in the ISFET in both sub- and superthreshold. Again, just as expected in chapters 2 and 3. The models describe the behaviour very accurately as the only thing not represented in the model is the decrease in slope in superthreshold for the transconductance. The simulations also showed all of the observed characteristics.

5.1.3 ph Trends for the Reference Voltage, Current and Transconductance

Reference Voltage pH trend

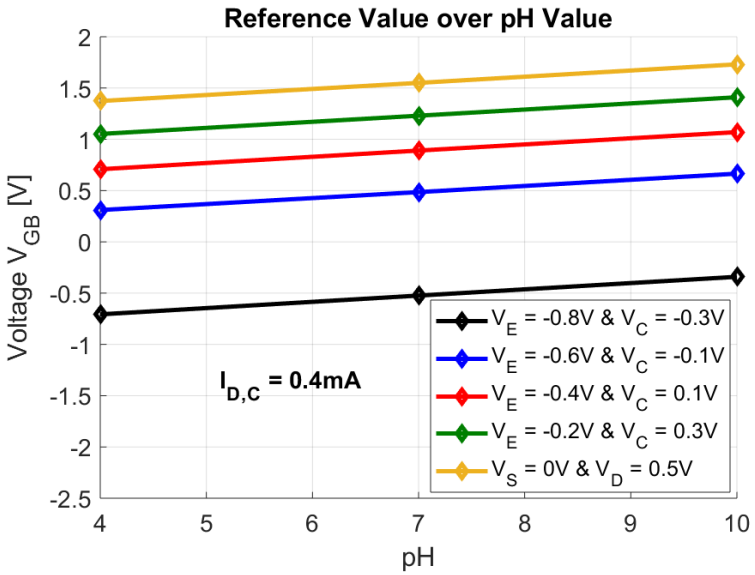

Figure 5.9: ISBIT measurement reference value over pH.

In figure 5.9 the gate-bulk voltage is plotted for each pH value. It if referred to as reference value, because the ISFET interacts directly with the buffer solution and not with the applied gate-bulk voltage, eq. 2.8. When a constant current value is assessed, it becomes apparent that the reference value increases for a higher pH value. Hence, a better response for relatively basic solutions rather than neutral or relatively acidic. An average increase of approximately $59.9mV$ was determined. Also, the reference value improves every time the emitter potential is decreased, hence, better for the ISBIT than for the ISFET.

Current pH trends

In figure 5.10, it can be seen that across all pH values the current in subthreshold stays comparably constant. However, because of the mentioned fluctuations in 5.1.1 and 5.1.2, the current for pH = 7 appears to be higher. Anyways, at $V_{GB} = -2V$ generally the current has increased every time the more negative V_E becomes, so, it can be said that it has improved in the ISBIT in comparison with the ISFET.

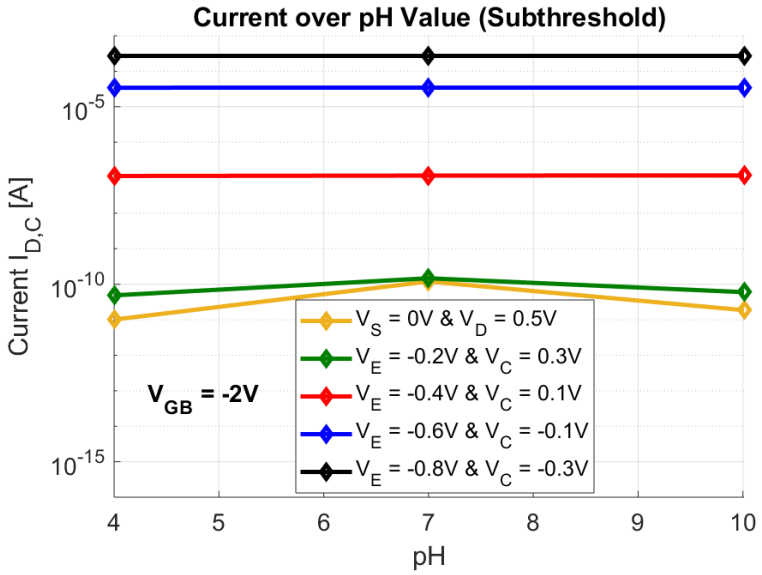

Figure 5.10: ISBIT measurement current over pH.

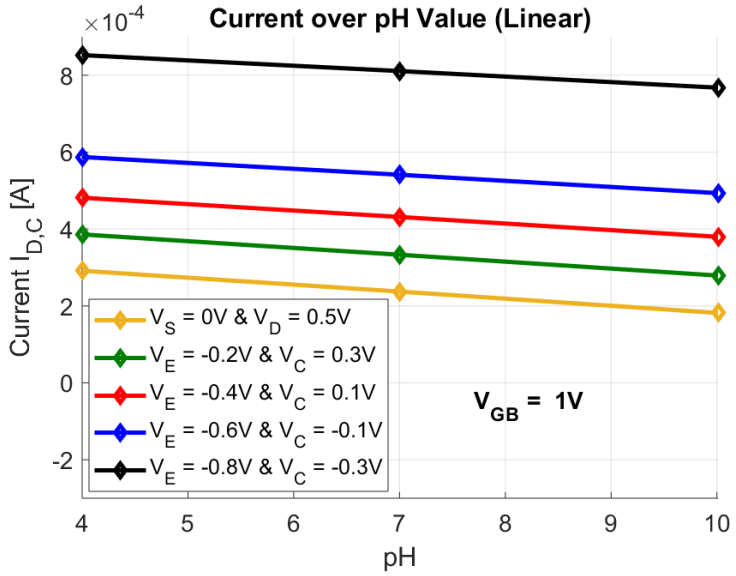

Figure 5.11: ISBIT measurement current over pH.

Figure 5.11 shows the trend for the drain and collector current over each of the three pH values of 4, 7 and 10.01. This was data was processed with a constant V_{GB} value of $1V$. Generally, it can be said that the current decreases when the pH value increases. Hence, the current is higher for relatively acidic solutions than neutral solutions and even higher than relatively basic solutions. But, the current increases for each decrease in emitter potential. So, overall the current response has been improved from the ISFET to the ISBIT, just like in subthreshold.

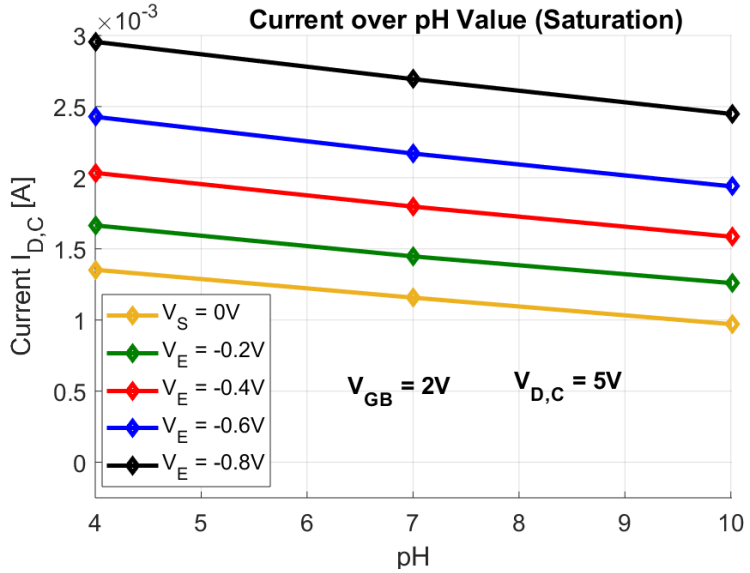

Figure 5.12: ISBIT measurement current over pH.

In superthreshold of the saturation operating region the current also increases in the ISBIT configuration for all pH values and all emitter potentials, which can be observed in figure 5.12. As in the linear operating region, though, the current decreases over the span of the pH values as it is higher for acidic solutions than for the other two.

Transconductance pH trends

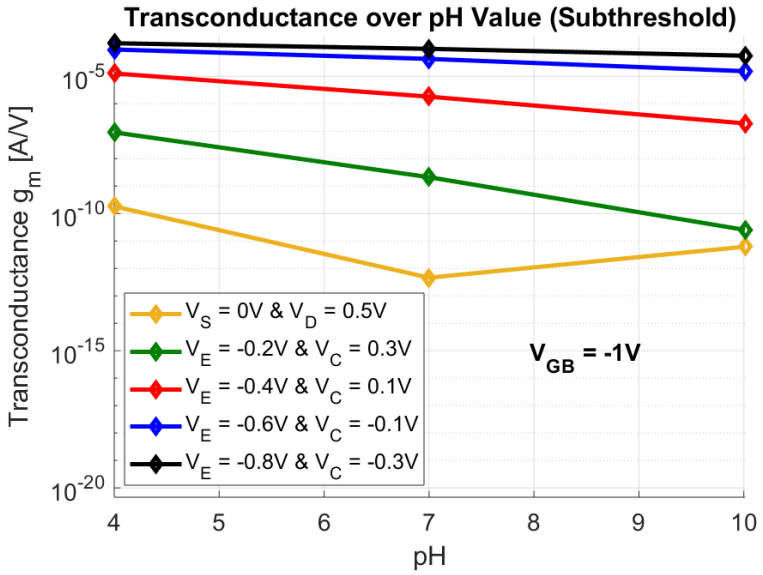

Figure 5.13: ISBIT measurement transconductance over pH.

Figure 5.13 displays the transconductance in subthreshold across all pH values. The fluctuations again made it hard to determine exact values, but generally it can be said that the transconductances decreases from $pH = 4$ to $pH = 10.01$. Also, it can be seen that g_m improves in the ISBIT configuration, i.e the higher the transconductance the lower the supplied emitter bias voltage.

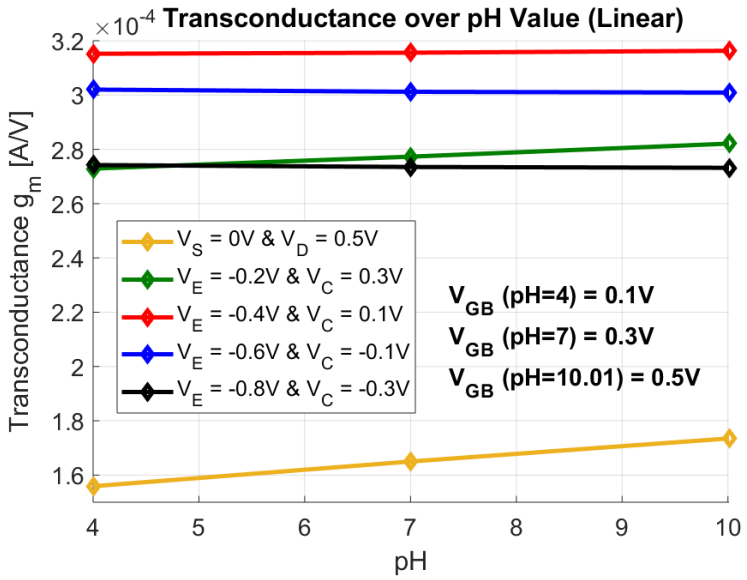

Figure 5.14: ISBIT measurement transconductance over pH.

In superthreshold of the linear operating region the transconductance trend was hard to assess, as can be seen in figure 5.14. The gate-bulk voltage had to be shifted to get a direct comparison of the graphs, because the transconductance shifted every time. If this weren't done then the values would sometimes be in subtreshold and thereby preventing a good comparison. So, the only aspect that can be taken from the figure is that the transconductance doesn't increase significantly except for the difference in threshold voltage between all of them. Again, the shift in threshold is caused by the emitter potential.

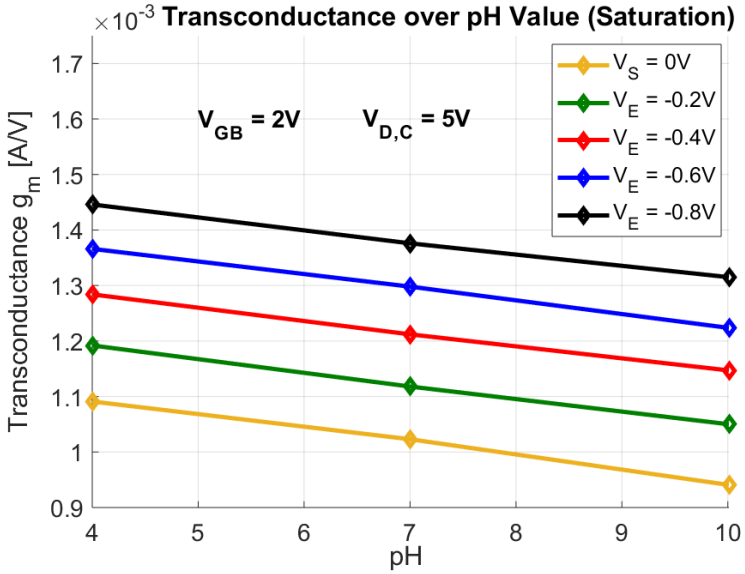

Figure 5.15: ISBIT measurement transconductance over pH.

In superthreshold of the saturation operating region, though, the transconductance improves for the ISBIT. This is shown in figure 5.15. Gradually, for increasing pH value, the transconductance g_m decreases. At a constant gate-bulk voltage of $2V$ the transconductance is higher for every decrease of V_E.

Chapter 6

Conclusions and Recommendations

This chapter consists of two sections. One answering the proposed goals and research question of Chapter 1 and one that makes recommendations as far as things that could have been done differently, ways of improvement for the presented research if it were repeated and appropriate questions for future research starting from what is presented here are concerned.

6.1 Conclusions

To simplify answering the research question, the different conclusions are made for the current, the transconductance and the general case.

Current

On the basis of the theoretical aspects, the simulations and obviously the measurement results it was determined that indeed the output current can be improved in the subthreshold-, linear- and saturation operating region. While the subthreshold current in the ISBIT showed a major increase in comparison with the ISFET, the linear and saturation superthreshold current showed a respectable improvement.

Transconductance

In terms of transconductance this was only determined for the subthreshold and saturation case. Even though fluctuations were visible, the subthreshold transconductance had a significant increase from the ISFET to the ISBIT in the exponential increase towards the threshold voltage. In saturation the increase was just minor, but nonetheless an improvement. In the linear operating region, however, only an increase near the threshold voltage was observed and otherwise even a reduction could be seen, after passing their respective maximum transconductance.

General

The general conclusion that can be drawn from this research is that the output parameters of an ISFET can be improved with the ISBIT configuration, but only to a certain extent as described above. This implies that indeed the sensitivity of an ISFET, without changing the method of measuring nor the structure and only by applying a bias voltage on the emitter terminal, can be increased in general terms.

6.2 Recommendations

One thing that could have been done differently was to include the source or rather emitter current in every measurement, such that this data could have also been processed. This is to purely see the effects of the interaction between emitter and body terminal on every measurement. However, a current measurement of source/emitter and bulk current is attached in appendix B. It was done for the general current capabilities of each device and not specifically for each measurement. Another thing that should have been considered more is the fact that semiconductors are prone to light and hence during the exchange of MOSFETs and ISFETs the waiting period before proceeding with the measurements should have been extended. This is to exclude any influence of light and hence assure that the results are not tainted.

Bibliography

[1] H. Ikink, "Sensoren," 1995. [Online]. Available: https://www.trouw.nl/home/sensoren~ad3628d7/

[2] W. Olthuis, *6 The ISFET principle of operation, 7 The ISFET experimental, 8 The ISFET some advanced applications*. W.Olthuis, 1995.

[3] P. Bergveld, "Thirty years of isfetology what happened in the past 30 years and what may happen in the next 30 years," *Sensors and Actuators*, vol. B88, pp. 1–20, 2003.

[4] R. J. E. Hueting, *An Initial Study of the Electrical Performance in the Low Injection Regime for Novel Ion-Sensitive Electron Devices*. University of Twente, 2011.

[5] R. J. Hueting, "Transconductanceisfetvsisbit," Private Communication, 2018.

[6] S. Verdonckt-Vandebroek, P. K. Ko, J. C. S. Woo, and S. S. Wong, "High-gain lateral bipolar action in a mosfet structure," *IEEE Transactions on Electron Devices*, vol. 38, no. 11, pp. 2487–2496, 1991.

[7] N. Arora, *MOSFET Modeling for VLSI Simulation: Theory and Practice*. World Scientific Publishing CO. Pte. Ltd., 1993.

[8] R. J. E. Hueting, *Semiconductor Devices Explained More*. Faculty EEMCS, University of Twente, 2018.

[9] H. Yuan, H.-C. Kwon, S.-H. Yeom, D.-H. Kwon, and S.-W. Kang, "Mosfet-bjt hybrid mode of the gated lateral bipolar junction transistor for c-reactive protein detection," *Biosensors and Bioelectronics*, vol. 28, pp. 434–437, 2011.

[10] S. Verdonckt-Vandebroek, J. You, J. C. S. Woo, and S. S. Wong, "High-gain lateral p-n-p bipolar action in a p-mosfet structure," *IEEE Transactions on Electron Devices*, vol. 13, no. 6, pp. 312–313, 1992.

Appendix A

Remaining MOSFET/MOSBIT Measurements

A.1 MOSFET and MOSBIT middle

A.1.1 Linear Operating Region

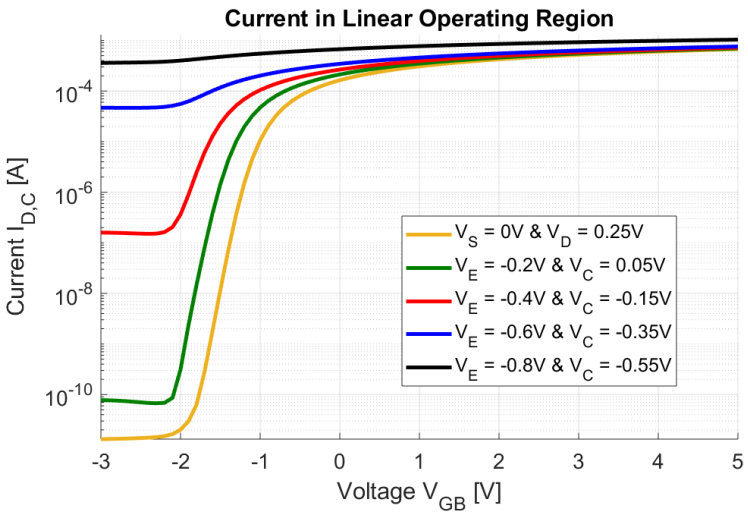

Figure A.1: MOSFET measurement in linear operating region logarithmic scale

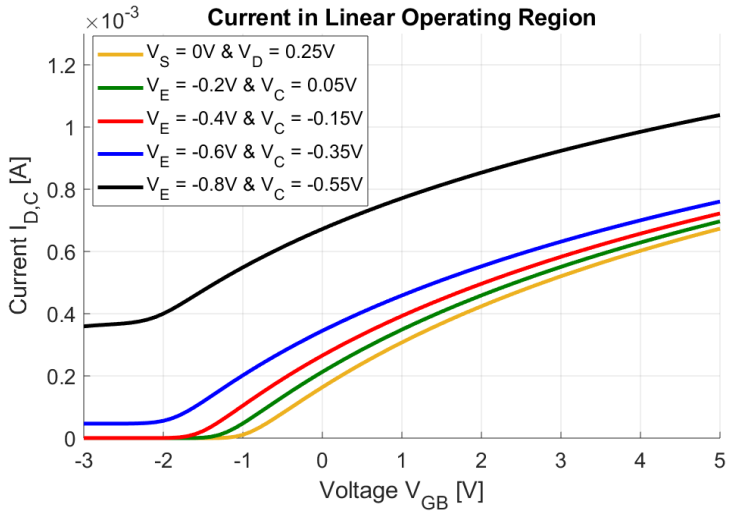

Figure A.2: MOSFET measurement in linear operating region

MOSFET Transconductance Linear

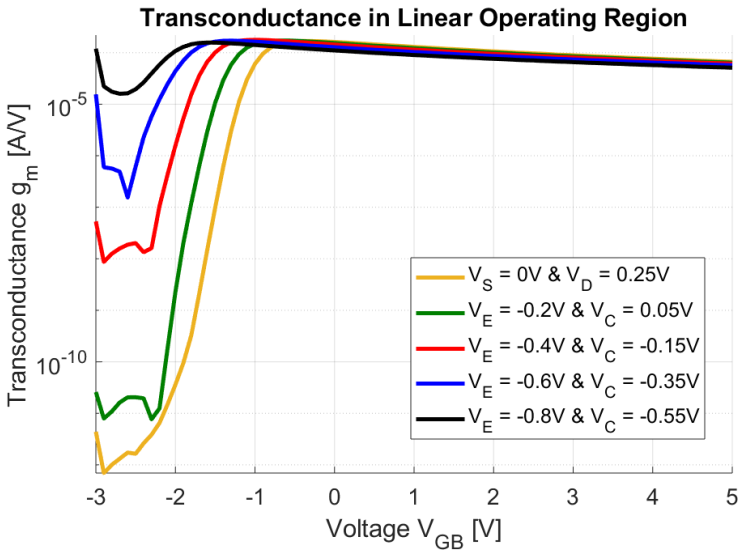

Figure A.3: MOSFET measurement transconductance in linear operating region logarithmic scale

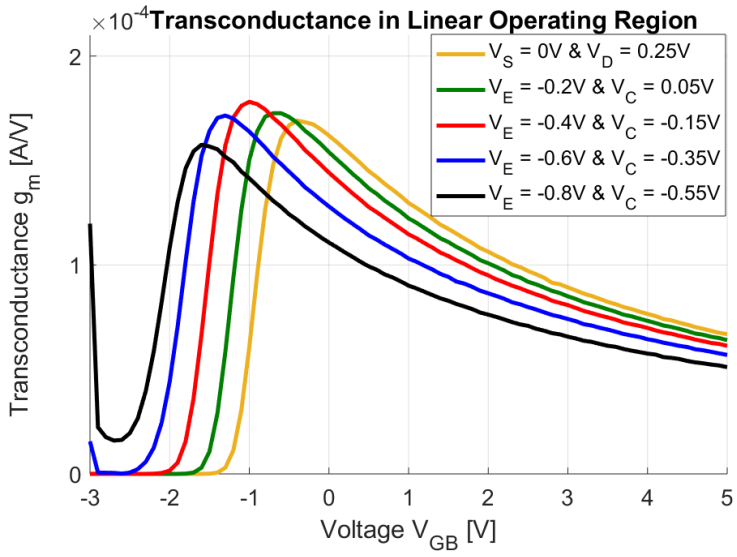

Figure A.4: MOSFET measurement transconductance in linear operating region

A.1.2 Saturation Operating Region

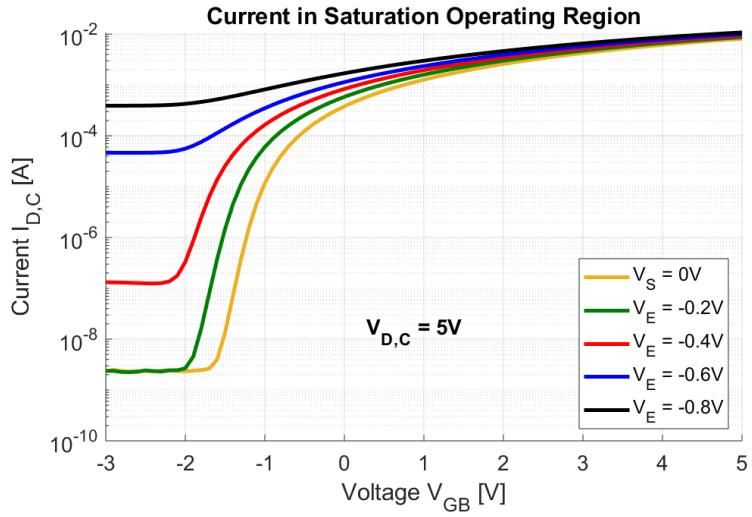

Figure A.5: MOSFET measurement in saturation operating region logarithmic scale

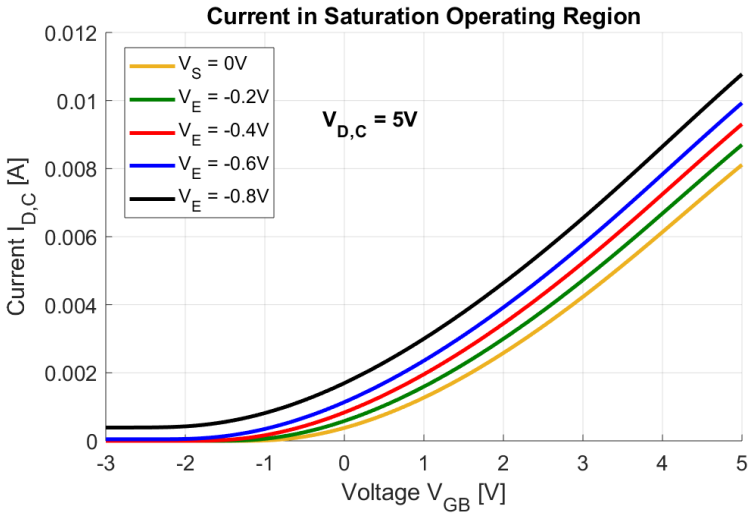

Figure A.6: MOSFET measurement in saturation operating region

MOSFET Transconductance Saturation

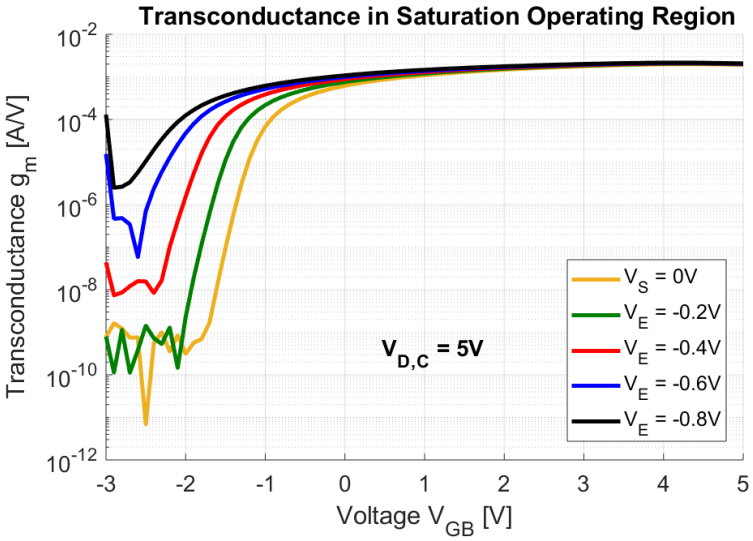

Figure A.7: MOSFET measurement transconductance in saturation operating region logarithmic scale

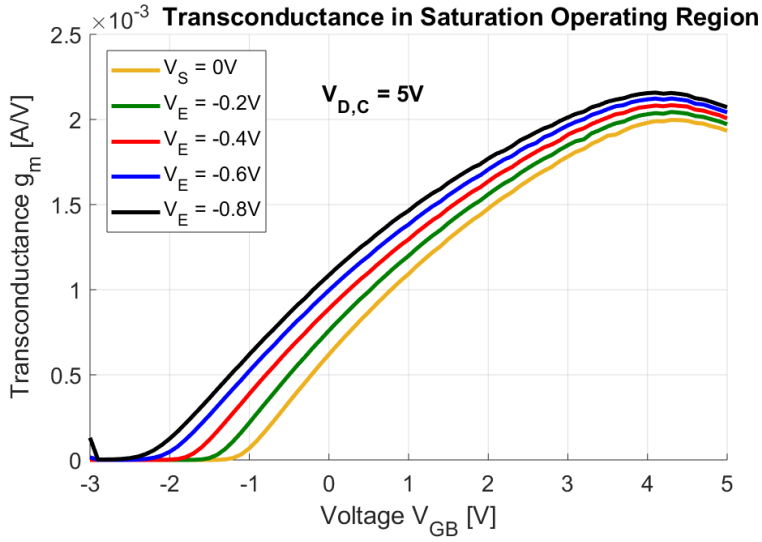

Figure A.8: MOSFET measurement transconductance in saturation operating region

A.1.3 Linear but non constant vds

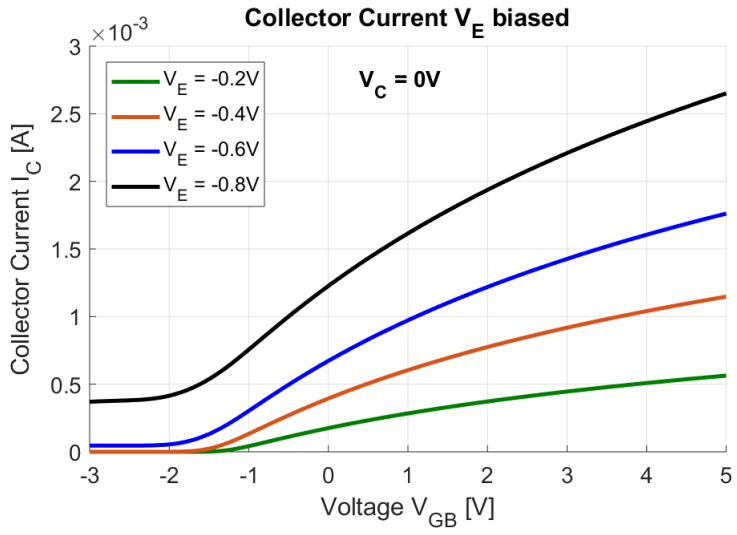

Figure A.9: MOSFET measurement linear vds variable

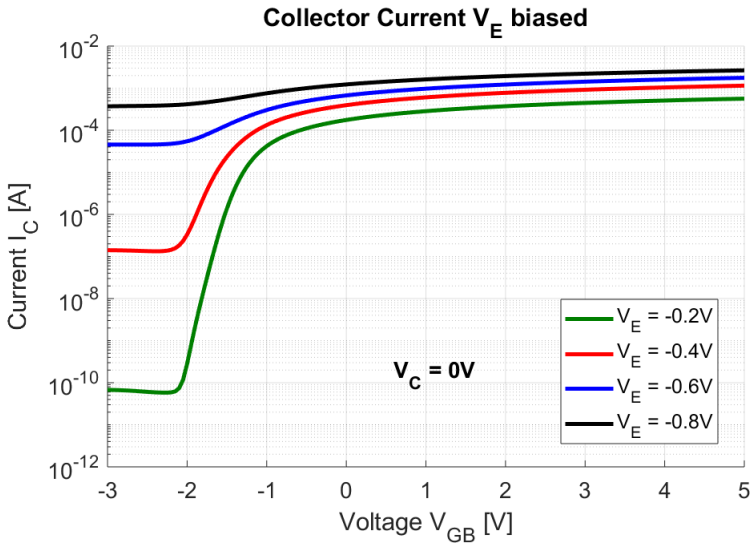

Figure A.10: MOSFET measurement linear vds variable log

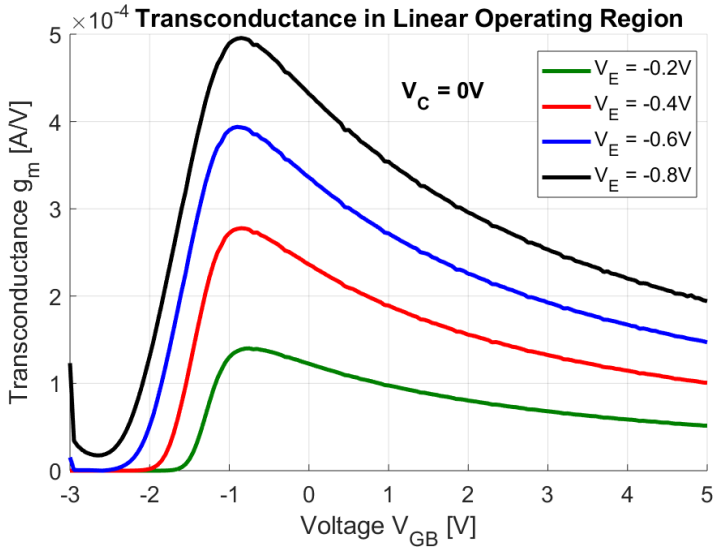

Figure A.11: MOSFET measurement linear vds variable trans

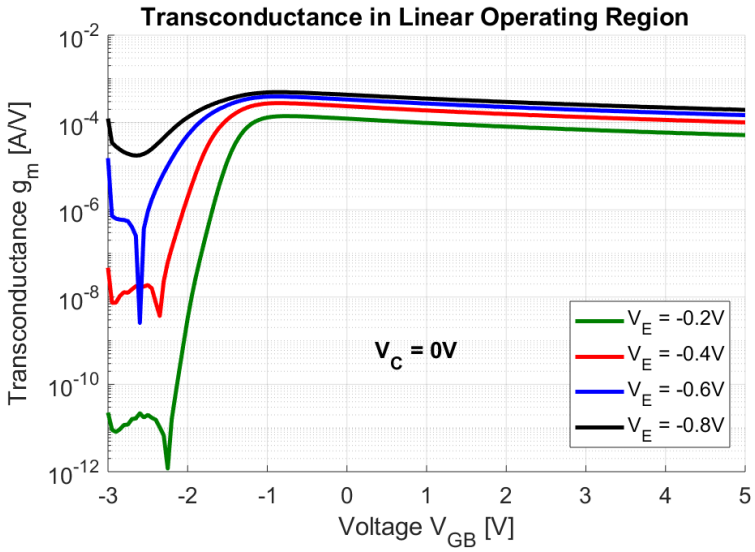

Figure A.12: MOSFET measurement linear vds variable trans log

A.1.4 Id-Vds and Diode relation

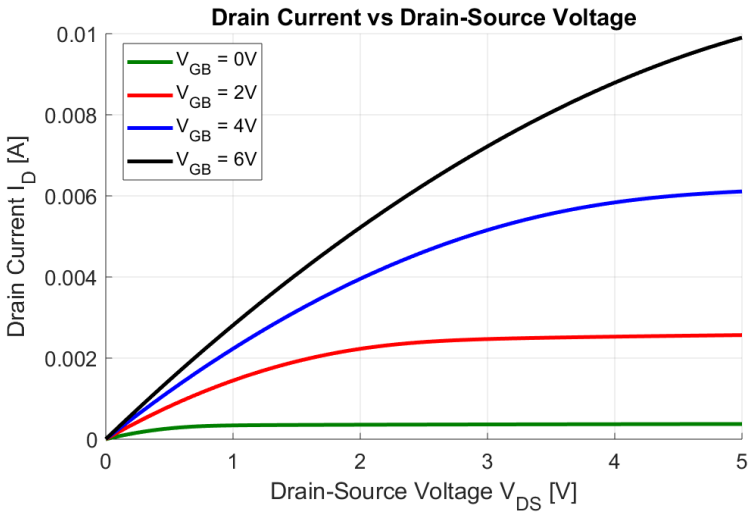

Figure A.13: MOSFET measurement IDVDS

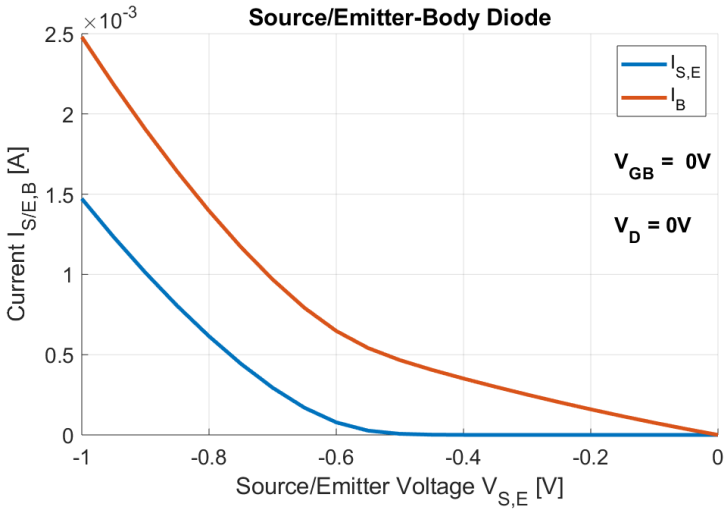

Figure A.14: MOSFET measurement Diode

Appendix B

Remaining ISFET/ISBIT measurements

B.1 ISFET and ISBIT remaining ph=4 measurements

B.1.1 Non constant vds

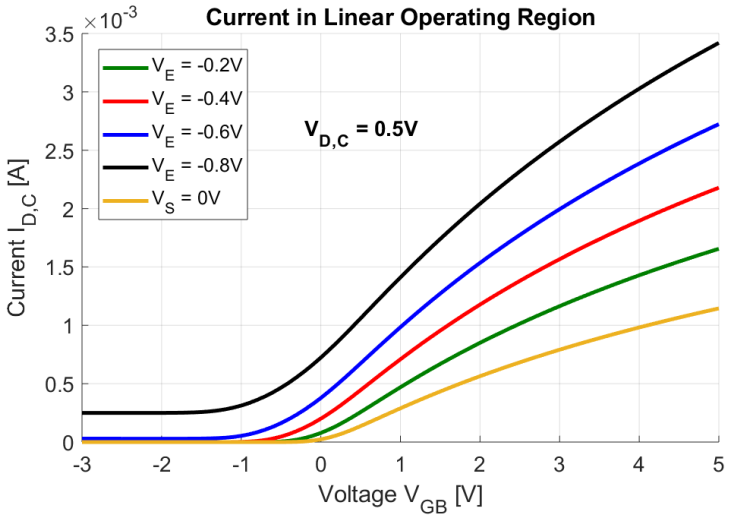

Figure B.1: ISFET measurement in linear operating region linear scale

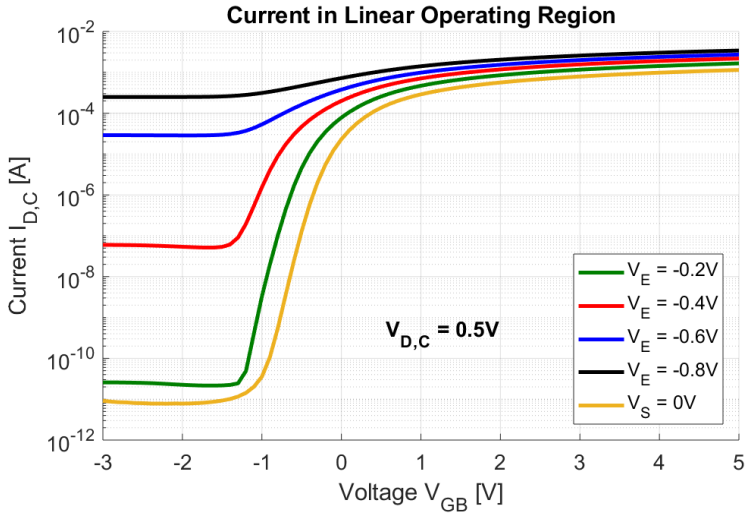

Figure B.2: ISFET measurement in linear operating region logarithmic scale

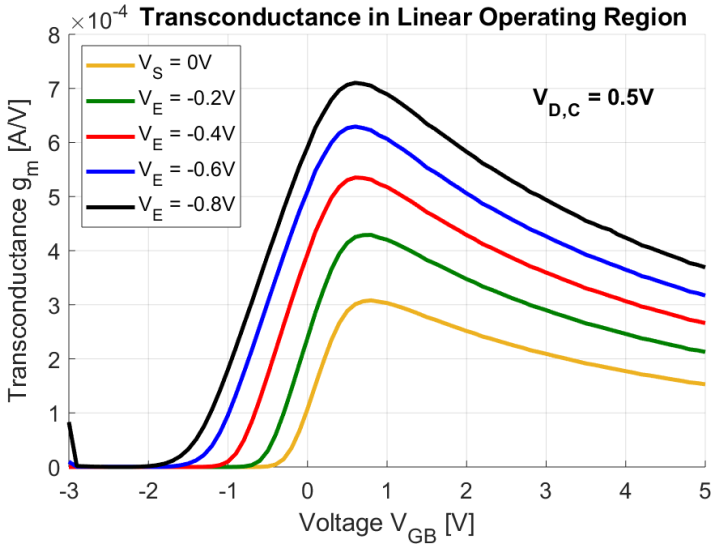

Figure B.3: ISFET measurement transconductance in linear operating region linear scale

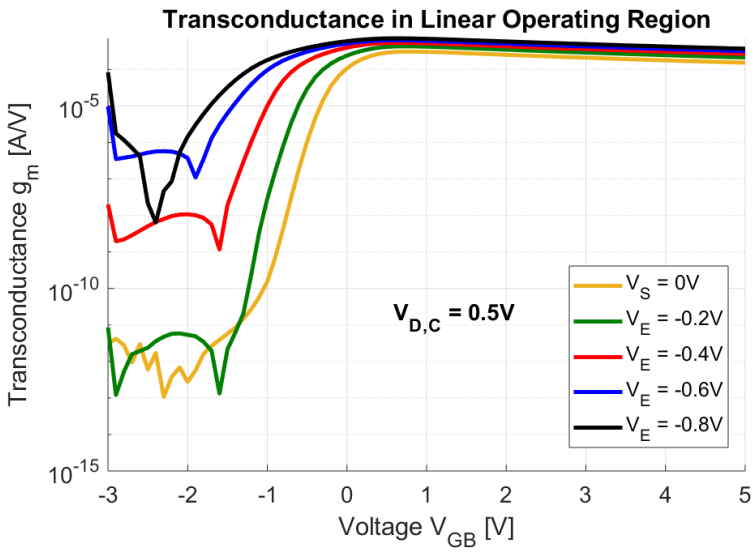

Figure B.4: ISFET measurement transconductance in linear operating region logarithmic scale

B.1.2 Id-Vds and Diode relation

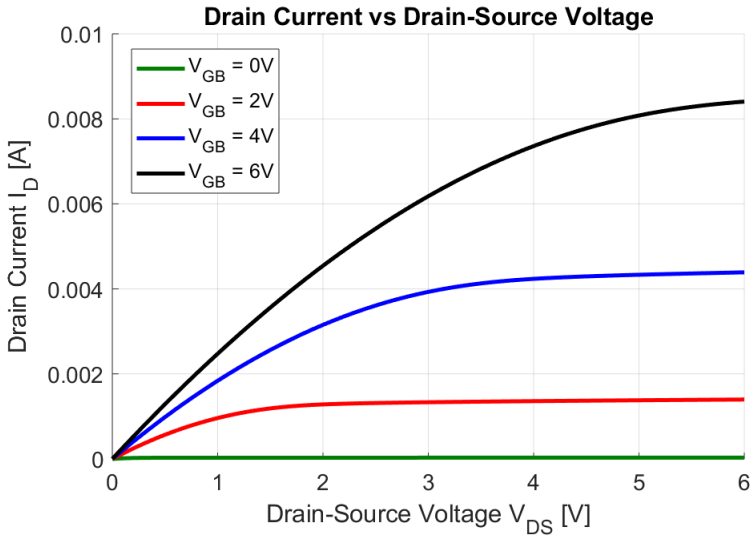

Figure B.5: ISFET measurement IDVDS 4pH

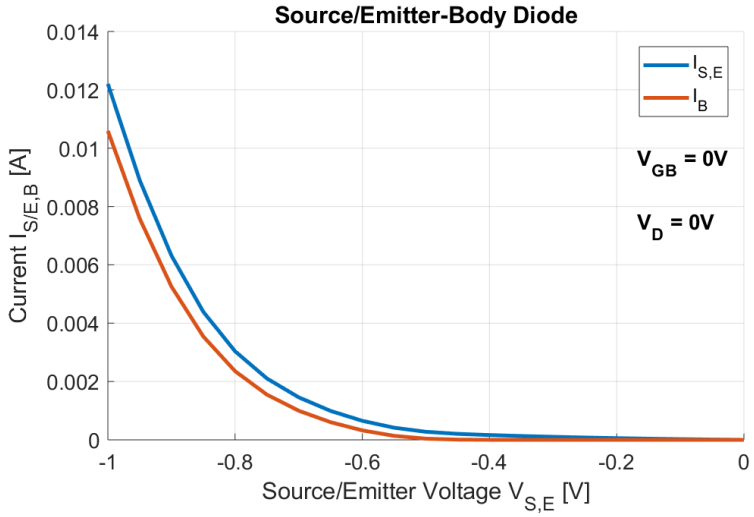

Figure B.6: MOSFET measurement Diode 4pH